Cooling the Envelopes of Gas Giants

Accretion, structure formation and observability

Schulik, Matthäus

2020

Document Version:
Publisher's PDF, also known as Version of record

Cooling the envelopes of Gas Giants

Accretion, Structure formation and observability

MATTHÄUS SCHULIK
DEPT. OF ASTRONOMY AND THEORETICAL PHYSICS | LUND UNIVERSITY 2020

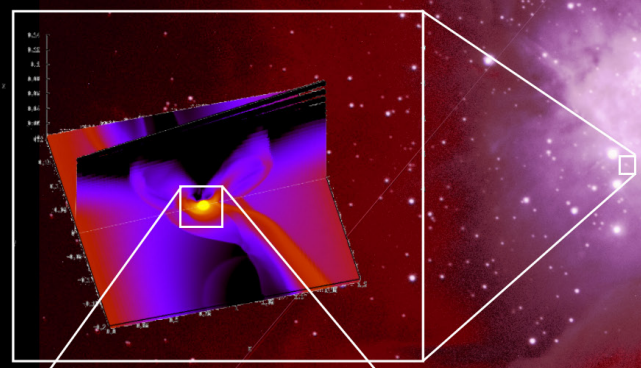

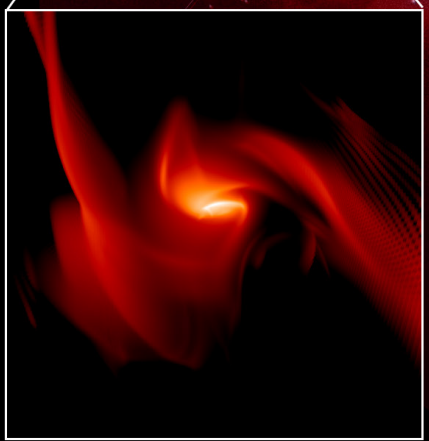

Printed by Media-Tryck, Lund 2020 NORDIC SWAN ECOLABEL 3041 0903

Faculty of Science
Department of Astronomy
and Theoretical Physics

ISBN 978-91-7895-480-3

Cooling the envelopes of gas giants

Matthäus Schulik

LUND
UNIVERSITY

Thesis for the degree of Doctor of Philosophy

Thesis advisors: Prof. Dr. Anders Johansen, Dr. Bertram Bitsch,
Dr. Michiel Lambrechts
Faculty opponent: Prof. Dr. Wilhelm Kley

To be presented, with the permission of the Faculty of Science of Lund University, for public criticism in the Lundmark lecture hall (Lundmarksalen) at the Department of Astronomy and Theoretical Physics on Friday, the 15th of May 2020 at 09:00.

Organization
LUND UNIVERSITY
Department of Astronomy and Theoretical Physics
Box-43
SE-22100 Lund, Sweden

Document name
DOCTORAL DISSERTATION
Date of issue

Author(s)
Matthäus Schulik

Sponsoring organization

Title and subtitle
Cooling the Envelopes of Gas Giants – Accretion, structure formation and observability

Abstract

We know now that discs of gas and dust, so-called protoplanetary discs, form planets as side-products of the naturally occurring star formation process throughout the Milky Way. Young, growing planets in such discs are commonly referred to as protoplanets. In about 10\% of the so-far observed stars, this planet formation process leads to the occurrence of giant planets, such as Saturn, Jupiter, or even more massive ones. During their early growth, protogiants are expected to be enshrouded in an extremeley extended atmosphere which is still connected to the parent disc, called the envelope. This envelope controls the inflow of mass as well as the cooling properties of the protogiant and later collapses to provide most of the mass of the planet itself. The planetary systems hosting those planets during their envelope growth are tremendously affected by them, be it through their influence on the gas and dust reservoir for further planet formation, or during the late dynamical evolution of the entire planetary system. Due to those factors it is important to know how rapidly and under which protoplanetary disc conditions gas giant envelopes grow.

During my thesis, I used a state-of-the-art simulation code in order to study the growth process, structures and observability of the extended gaseous envelopes of those young planets. At first, I had to solve significant numerical and technical difficulties in order to begin simulating the growth of gas giants. Overcoming those led to a requirement for the numerical resolution of envelopes in order to yield correct growth rates. Subsequently, I was able to simulate a full mass sequence, following protoplanetary growth from Neptune-mass planets up to Jupiter-mass giants. Those simulations show short overall growth timescales for gas giants ranging from hundreds to tens of thousands of years, whereas circumplanetary discs disappear on timescales of a few million years. Hereby it is the growth of dust acting to accelerate this process as large dust cools envelopes efficiently. This emphasizes that the most time-consuming process in nature must be the assembly of a gas giant's solid core.

Furthermore, my work shows that the cooling capability provided to envelopes by dust particles of millimeter-sizes will lead to the formation of circumplanetary discs. These are discs which orbit their host planet and are thought to be the birth sites of regular moon systems around giant planets. During the last episode of my research I compared my simulation data with actual observations of the protoplanet-hosting PDS 70 system. The latter results confirm the presence of a suspected circumplanetary disc around PDS 70c. I further find that the width of the protoplanetary spectrum can be explained by a population of dust grains that have grown significantly to sizes of millimeters.

Key words
Planet formation, Gas giants, Hydrodynamics

Classification system and/or index terms (if any)

Supplementary bibliographical information

Language
English

ISSN and key title

ISBN
978-91-7895-480-3 (Print)
978-91-7895-481-0 (pdf)

Recipient´s notes

Number of pages
159

Price

Security classification

Distribution by (name and address)

Signature  Date 2020 – 04 – 02

Cooling the envelopes of gas giants

Accretion, structure formation and observability

Matthäus Schulik

LUND
UNIVERSITY

Faculty Opponent

Prof. Dr. Wilhelm Kley
Department of Physics and Astronomy
Universität Tübingen, Germany

Evaluation Committee

Dr. Farzana Meru
Department of Physics
University of Warwick, UK

Prof. Dr. Christoph Mordasini
Physikalisches Institut
Universität Bern, Switzerland

Dr. Simon Albrecht
Department of Physics and Astronomy
Aarhus University, Denmark

Cover: Image of the Great Nebula M42 in Orion taken with the LMK-telescope at Lunds University, in B, R and I filters. M42 is a region of active star and planet formation, with stellar isochronic ages ranging from 1-3 million years. The first zoom inset is centered on the protoplanetary disc around V* V2423 Ori. The inset shows a simulated example 3-D density data set from one of the giant protoplanetary envelopes described in this thesis. The second inset shows the same, as post-processed synthetic observation with silicate dust as opacity source, at a wavelength of 8 μm. The protoplanet is enshrouded in mystery by the envelope formed via the action of its own gravity.

Faculty of Science, Department of Astronomy and Theoretical Physics
ISBN: 978-91-7895-480-3 (print)
ISBN: 978-91-7895-481-0 (pdf)

Printed in Sweden by Media-Tryck, Lund University, Lund 2020

Media-Tryck is a Nordic Swan Ecolabel certified provider of printed material. Read more about our environmental work at www.mediatryck.lu.se
MADE IN SWEDEN

Dedykowane do mojich rodziców, które mi umożliwili te życie.

The truth always carries the ambiguity of the words used to express it.

Frank Herbert, God emperor of Dune

We must know. We will know.

David Hilbert, Finalizer to his speech to the German Society of Scientists and Physicians, 1930

Contents

List of publications

This thesis is based on the following publications:

I **Global 3D radiation-hydrodynamic simulations of gas accretion: The opacity dependent growth of Saturn-mass planets**

M. Schulik, A. Johansen, B. Bitsch, and E. Lega (2019)
Astronomy & Astrophysics, vol. 632, A118 (23 p.)

II **On the structure and mass delivery towards circumplanetary discs**

M. Schulik, A. Johansen, B. Bitsch, E. Lega and M. Lambrechts (2020)
Accepted in Astronomy & Astrophysics (19 p.)

III **The influence of dust growth on the observational properties of circumplanetary discs**

M. Schulik, A. Johansen, B. Bitsch, and M. Lambrechts (2020)
Submitted to Astronomy & Astrophysics (13 p.)

Popular summary in English

Astronomy and astrophysics finds itself in a time of great discoveries. Whereas for most of the timeline of human civilisation we were left with lingering questions about the origins and uniqueness of our solar system, we are now slowly breaching through the shroud of ignorance clouding some of the oldest mysteries. In this endeavour to understand our place in the universe, the last decades have seen the rapid development of two subbranches of astronomy and astrophysics, namely that of the study of the formation of planets and that of the studies of newly discovered exoplanets.

We know now that discs of gas and dust, so-called protoplanetary discs, form planets as side-products of the naturally occurring star formation process throughout the Milky Way. Young, growing planets in such discs are commonly referred to as protoplanets. In about 10% of the so-far observed stars, this planet formation process leads to the occurrence of giant planets, such as Saturn, Jupiter, or even more massive ones. During their early growth, protogiants are expected to be enshrouded in an extremeley extended atmosphere which is still connected to the parent disc, called the envelope. This envelope controls the inflow of mass as well as the cooling properties of the protogiant and later collapses to provide most of the mass of the giant planet itself. The planetary systems hosting those planets during their envelope growth are tremendously affected by them, be it through their influence on the gas and dust reservoir for further planet formation, or during the late dynamical evolution of the entire planetary system. Due to those factors it is important to know how rapidly and under which protoplanetary disc conditions gas giant envelopes grow.

During my thesis, I used a state-of-the-art simulation code in order to study the growth process, structures and observability of the extended gaseous envelopes of those young planets. At first, I had to solve significant numerical and technical difficulties in order to begin simulating the growth of gas giants. Overcoming

those led me to formulate a requirement for the numerical resolution of envelopes in order to yield correct growth rates. Subsequently, I was able to simulate a full mass sequence, following protoplanetary growth from Neptune-mass planets up to Jupiter-mass giants. Those simulations show short overall growth timescales for gas giants ranging from hundreds to tens of thousands of years, whereas circumstellar discs disappear on timescales of a few million years. Hereby it is the growth of dust acting to accelerate this process as large dust cools envelopes efficiently. This emphasizes that the most time-consuming process in nature must be the assembly of a gas giant's solid core.

Furthermore, my work shows that the cooling capability provided to envelopes by dust particles of millimeter-sizes will lead to the formation of circumplanetary discs. These are discs which orbit their host planet and are thought to be the birth sites of regular moon systems around giant planets. During the last episode of my research I compared my simulation data with actual observations of the protoplanet-hosting PDS 70 system. The latter results confirm the presence of a suspected circumplanetary disc around PDS 70c. I further find that the width of the protoplanetary spectrum can be explained by a population of dust grains that have grown significantly to sizes of millimeters.

Those findings advance our understanding of planet formation by painting a self-consistent picture of the growth, structure formation and spectral properties of gas giant envelopes.

Populärvetenskaplig sammanfattning på svenska

Astronomin och astrofyik befinner sig i en tid full av stora upptäckter. Medan vi under den största delen av mänsklighetens historia har undrat över vårt ursprung och över hur unikt vårt solsystem är, tar vi oss nu långsamt igenom okunnighetens slöja som döljer några av de äldsta mysterierna. I denna strävan att förstå vår plats i universum har två nya undergrenar till astronomi och astrofysik utvecklats snabbt under de senaste årtiondena; studier av planetbildning och av nyupptäckta exoplaneter.

Vi vet nu att skivor av gas och stoft, så kallade protoplanetära skivor, bildar planeter som biprodukter av de stjärnbildningsprocesser som sker naturligt i Vintergatan. Unga, växande planeter i sådana skivor kallas vanligtvis för protoplaneter. Kring ungefär 10% av de hittills observerade stjärnorna leder planetbildningsprocessen till förekomsten av jätteplaneter, såsom Saturnus, Jupiter, eller till och med ännu mer massiva planeter. Under den tidiga tillväxtfasen förväntas protojättar vara omgivna av en vidsträckt atmosfär som fortfarande är förbunden med den protoplanetära skivan. Detta gashölje kontrollerar inflödet av massa och protojättens avsvalningsmöljigheter, samt kollapsar senare och ger då merparten av planetens massa. Planetsystemen som står värd för planeterna då deras gashölje växer påverkas kraftigt av detta, antingen genom påverkan på mängden gas och stoft som finns tillgängligt för vidare planetbildning, eller vid den senare dynamiska utvecklingen av hela planetsystemet. På grund av dessa faktorer är det viktigt att veta hur snabbt och under vilka förutsättningar gasjättars höljen växer.

I min avhandling använde jag toppmoderna datormodeller för att studera tillväxtprocesser, strukturer och observationsmöljigheter för dessa unga planeters gashöljen. Jag behövde först lösa signifikanta numeriska problem och tekniska svårigheter för att kunna påbörja simuleringar av gasjättarnas tillväxt. Detta ledde

till att jag formulerade ett krav på numerisk upplösning av planeternas gashöljen för att ge korrekt tillväxthastighet. Därefter kunde jag simulera en hel massekvens, där jag följde den protoplanetära tillväxten för gasjätteplaneter från Neptunus till Jupiters storlek. Dessa simuleringar visar att gasjättar växer snabbt, under hundratill tusentals år, medan det tar miljontals år för den cirkumplanetära gas- och stoftskivan att försvinna. Det är alltså det växande stoftet som accelerar processen då större stoftkorn effektivt kyler ner gashöljet. Detta understryker att den komplicerade processen i naturen bör vara uppbyggnaden av gasjättarnas fasta kärnor.

Dessutom har min avhandling visat att nedkylningskapaciteten som gashöljena får av millimeterstora stoftpartiklar leder till bildandet av cirkumplanetära skivor. Detta är skivor som kretsar runt värdplaneten och där man tänker sig att jätteplaneternas reguljära månsystem bildas. Under den sista delen av min forskning försökte jag jämföra data från mina simuleringar med faktiska observationer av PDS 70, ett värdsystem för protoplaneter. De senare resultaten bekräftar misstankar om en cirkumplanetär skiva runt PDS 70c. Jag finner också att bredden på protoplanetens spektrum kan förklaras av en stoftpopulation som växt till betydande storlek, runt en millimeter.

Dessa rön avancerar vår förståelse av planetbildning genom att ge en fristående bild av tillväxt, strukturbildning och spektrala egenskaper för gasjättars höljen.

Przystępnie sformułowane podsumowanie w języku polskim

W chwili obecnej dwie dyscypliny nauki - astronomia i astrofizyka przeżywają okres wielkich odkryć. Przez większość swej egzystencji nasza ludzka cywilizacja zmuszona była zadowalać się pytaniami bez odpowiedzi czy też spekulacjami na temat genezy naszego Systemu Słonecznego i jego wyjątkowości. Powoli jednak nauka pozwala „uchylić rąbek tajemnicy" w tej kwestii. Dlatego też, aby lepiej zrozumieć nasze miejsce we wszechświecie, w ostatnich dekadach rozwinięto znacznie podległe astronomii i astrofizyce dyscypliny naukowe takie jak badania nad powstawaniem planet i badania nowo odkrytych planet pozasłonecznych zwanych inaczej egzoplanetami.

Obecnie wiemy już, że planety powstają z dysków składających się z gazu i pyłu kosmicznego, tak zwanych dysków protoplanetarnych, które tworzą się w naszej Galaktyce jako produkt uboczny powstawania gwiazd. Te młode twory zwane są protoplanetami. Około 10% obserwowanych dysków prowadzi do powstania gazowych olbrzymów takich jak Saturn, Jowisz czy nawet jeszcze potężniejszych. Przyjmuje się, że we wczesnej fazie powstawania protoplaneta posiada ekstremalnie rozrzedzoną atmosferę gazową, która łącząc się z dyskiem protoplanetarnym tworzy rozległą otoczkę. Kontroluje ona przepływ materii, odgrywa tym samym decydującą rolę w regulowaniu ochładzania protoplanety, aby w końcu ulec niekontrolowanemu procesowi sprężania i stać się zaczątkiem masy gazowego olbrzyma. Od tej chwili mamy już do czynienia z protoolbrzymem, a rosnące protoolbrzymy, podczas kiedy buduje się ich otoczka, wywierają ogromny wpływ na swoje macierzyste systemy planetarne poprzez wykorzystywanie rezerw gazów i pyłów, potrzebnych z kolei do budowy innych planet, oraz oddziaływując, w późniejszym czasie, na orbitalną dynamikę systemu. Te wszystkie czynniki podkreślają, jak ważne jest poznanie tempa i warunków powstawania gazowych olbrzymów.

W niniejszej rozprawie doktorskiej dla symulowania interesujących nas pro-

cesów użyto programu komputerowego na najwyższym poziomie nauki i techniki w celu zbadania i obliczenia prędkości rośnięcia, tworzenie struktur i właściwości obserwacyjnych w otoczkach protoolbrzymów. Rozpoczęto od rozwiązania poważnych problemów technicznych i numerycznych. W efekcie można było wyliczyć kompletną sekwencję wzrostu mas planetarnych, od mniejszych podobnych Neptunowi aż do wysoce masywnych takich typu Jowisza. Badania te wykazały stosunkowo krótki czas rośnięcia protoplanet mianowicie od dziesięciu tysięcy do stu tysięcy lat, przy czym dyski protoplanetarne cieszą się żywotnością rzędu kilku milionów lat. By przyśpieszy proces chłodzenia otoczki zostały wykorzystane w tej pracy znane już wcześniej wyliczenia, że im większe cząsteczki pyłu tym szybciej postępuje ochładzanie się otoczki. Obliczenia te wskazują, że w naturze najbardziej czasochłonny musi być proces tworzenia się samego twardego jądra gazowego olbrzyma.

Dalsze nasze badania wykazują, że prędkość ochładzania gazu przez pył o milimetrowych cząstkach, a więc stosunkowo dużych, prowadzi do powstania tak zwanych dysków okołoplanetarnych. Ten rodzaj dysków okrąża swoją planetę macierzystą, nie gwiazdę. Przypuszcza się, że w naszym Układzie Słonecznym w takich dyskach powstały regularne księżyce. W ostatniej fazie badań skupiono się na porównaniu własnych danych symulacyjnych z danymi obserwacyjnymi Systemu PDS 70, w którym to znajduje się młody gazowy olbrzym PDS 70c, i o którym się przypuszcza, że jest okrążany przez dysk okołoplanetarny, co z kolei potwierdzałoby wnioski wynikające z naszej pracy. Ponadto widmo emisyjne tej protoplanety wytłumaczyć można tylko posiadaniem przez nią cząstek pyłu o wielkości ok. milimetra. Te badania wzbogacają naszą wiedzę o protoplanetach przez wyciągnięcie spójnych wniosków na tematy tempa wzrostu, tworzenie struktur i właściwości obserwacyjnych w otoczkach protoolbrzymów.

Allgemeinverständliche Zusammenfassung auf Deutsch

Die Wissenschaftsdisziplin der Astronomie und Astrophysik befindet sich in einer Zeit großer Entdeckungen. Nachdem die menschliche Zivilisation sich für den Großteil ihrer Existenz mit mehr Fragen als Antworten begnügen musste, was den Ursprung und die Einmaligkeit unseres Sonnensystems betrifft, so wird so langsam der Schleier des Unwissens um manche dieser ältesten Fragen gelüftet. In diesem Unterfangen unseren Platz im Universum besser zu verstehen, haben zwei Teildisziplinen der Astronomie und Astrophysik, nämlich die Untersuchung von Planetenentstehung und die Erforschung von neu entdeckten Exoplaneten, in den letzten Jahrzehnten rasante Fortschritte gemacht.

Wir wissen nun, dass Planeten in Scheiben bestehend aus Gas und Staub entstehen, den sogenannten protoplanetaren Scheiben, welche sich als Nebenprodukte des natürlichen Sternenentstehungsprozesses in der gesamten Milchstraße bilden. Junge, heranwachsende Planeten in solchen Scheiben nennt man Protoplaneten. In ungefähr 10% dieser beobachteten Scheiben führen diese Prozesse der Planetenentstehung zur Bildung von Gasriesen wie Saturn, Jupiter oder gar Planeten noch höherer Massen. Während ihrer frühen Wachstumsphasen wird erwartet, dass Protoplaneten eine extrem ausgedehnte Atmosphäre besitzen, die mit der protoplanetaren Scheibe verbunden ist, welche oft als Hülle bezeichnet wird. Die Hülle kontrolliert den Massenfluss zum Protoplaneten, spielt eine entscheidende Rolle für seine Kühlung und fällt letztlich in sich zusammen, wodurch sie zum Hauptbestandteil der Masse eines Gasriesen wird. Planetensysteme, die solche Gasriesen während ihres Hüllenwachstums beherbergen, werden stark von ihnen geprägt, sei es durch ihren Einfluss auf das Gas- und Staubreservoir für die Bildung anderer Planeten oder durch spätere Beeinflussung der orbitalen Eigenschaften des gesamten Planetensystems. Aufgrund dieser Faktoren ist es wichtig

zu wissen wie schnell solche Gasriesen entstehen, und welche Bedingungen in der protoplanetaren Scheibe dafür entscheidend sind.

Während meiner Doktorarbeit habe ich einen Simulationscode auf dem neuesten Stand der Wissenschaft benutzt, um die Prozesse des Heranwachsens, der Entstehung von Strukturen und der Beobachtbarkeit dieser jungen Gasplaneten zu untersuchen. Als erster Schritt mussten technische und numerische Schwierigkeiten beseitigt werden, um die Simulationen des Planetenwachstums beginnen zu können. Die Überwindung dieser Probleme führte mich zur Formulierung eines numerischen Kriteriums, welches die Simulationen erfüllen müssen, um korrekte Wachstumsraten der protoplanetaren Gashüllen zu erhalten. Dies ließ mich eine komplette Abfolge von Planetenmassen simulieren, beginnend mit neptunähnlichen Planeten bis hin zu Gasriesen, welche mit Jupiter vergleichbar sind. Diese Simulationen zeigen vergleichsweise kurze Wachstumszeiten von zehntausend bis hundertausend Jahren, während protoplanetare Scheiben eine Lebensdauer von wenigen Millionen Jahren haben. Hierbei spielt das Wachstum von Staub eine beschleunigende Rolle, da Staubwachstum die Kühlungsraten der Hülle erhöht. Diese Zeitskalen lassen erkennen, dass in der Natur der zeitintensivste Prozess das Wachstum des festen Kerns der Gasriesen sein muss.

Meine weiterführende Arbeit zeigt auf, dass die Kühlungsraten von millimetergroßem Staub zur Entstehung von zirkumplanetaren Scheiben führt. Diese Art von Scheiben umkreist ihren Mutterplaneten und es wird angenommen, dass die regulären Monde der Gasriesen in unserem Sonnensystem in solchen Scheiben entstanden sind. In der letzten Phase meiner Forschung beschäftigte ich mich damit, meine Simulationsdaten mit Beobachtungen des Systems PDS 70 zu vergleichen. In diesem gibt es einen jungen Gasriesen, der möglicherweise von einer zirkumplanetaren Scheibe umkreist wird, worauf meine Arbeit hindeutet. Darüber hinaus scheint das Spektrum dieses Protoplaneten nur mit Staub erklärbar zu sein, der bereits zu Größen von circa einem millimeter angewachsen ist.

Diese Forschung bringt unser Verständnis voran, indem sie ein selbstkonsistentes Bild zeichnet vom Wachstum, Strukturentstehung und der Beobachtbaren Eigenschaften von Gasriesen und ihrer Hüllen entwickelt.

Cooling the envelopes of gas giants: Accretion, structure formation and observability

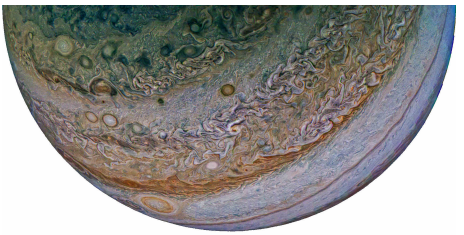

Chapter 1

Gas giants and their birth environments

The first reported observation of a planetary-mass companion around a G-type star, which is mostly remembered by the majority of the astronomical community and which led to last year's nobel prize (Mayor & Queloz 1995), stirred considerable scientific interest and quickly drowned the actually first reported exoplanets, which were presumably zombie-like pulsar planets (Wolszczan & Frail 1992).

The subsequent investigations of both types of objects revealed that nature seems to prefer to form planets around pre-main-sequence instead of post-supernova stars, an outcome greatly appreciated by the inhabitants of this planet and its scientific community, but one that dismayed the fans of exotic science-fictional scenarios.

Nonetheless, the mode of planet formation preferred by the local universe offers fascinating, yet unsolved puzzles. The author of this thesis hopes to give an appropriate treatment and brief overview to some of those puzzles where relevant, for the purpose of understanding the context of the articles contained at the end of this work.

1.1 Gas giant populations: Hot and Cold Jupiters

Since the first exoplanet discoveries, it became possible to extend the search parameters for exoplanets significantly. Planets or planetary candidates are found in large numbers by automated surveys in space (CoRoT, The Kepler Space telescope, Gaia, TESS) or on the ground (WASP, Trappist, HAT, NGTS, SPHERE)

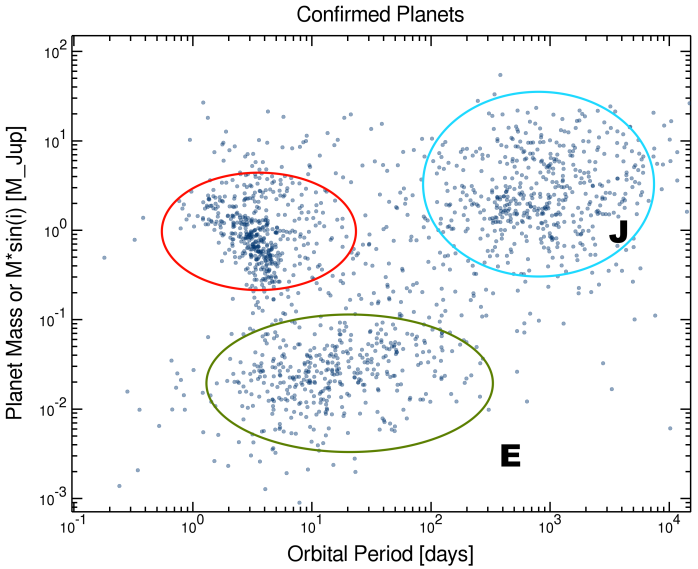

Figure 1.1: The current census of exoplanets with known or constrained masses. The ellipses mark significant clustering in this diagram which are commonly interpreted as populations of common physical origin. Super-Earth planets are delineated by the olive, hot Jupiters by the red and cold Jupiters by the blue ellipse. Note that this graph overrepresents the numbers in each individual population as e.g. hot Jupiter exoplanets are significantly easier to find than cold Jupiters. The lower right corner of the diagram is empty due to current instrumental limits. 'J' and 'E' indicate Jupiter and Earth, for comparison. ©Exoplanet archive/NASA/JPL-Caltech.

discovering planets around stars that are not limited to G-types. Every technique aimed at exoplanet discoveries has their own observational biases, most are more sensitive to massive and close-in planets. Those biases are reflected in the current population census of exoplanets with known or constrained masses, depicted in Figure 1.1, where on can read-off the three currently known large groups of exoplanets, hot Jupiters, cold Jupiters and Super-Earths.

Some parts of this diagram are not filled. While the bottom right corner is devoid of detections due to a severe lack of sensitivity for all techniques with survey capability, there are other voids in this diagram to which we assign physical mean-

ing today. Those other voids are thought to be leftovers from the past, encoding information about their mode of formation and subsequent evolution. The population of Super-Earths currently poses a mystery to us, as they seem to be present in about 50% of the planetary systems, and it is thought that their evolution into gas-giants should be efficient at the given masses (Ogihara & Hori 2018; Bitsch et al. 2019).

Furthermore, the giant planets, of which we presumably have a more complete picture, seem to separate significantly between the populations of Hot and Cold Jupiters. This separation has often been interpreted as a signature of gas-driven migration of giant planets during their formation. This gas-driven migration and the formation of gas giants has to occur in a large reservoir of gas, which we refer to as a circumstellar disc. The effect of the circumstellar disc on forcing protoplanets to change their semimajor axis, i.e. migrate, has been predicted long before exoplanets were discovered (Goldreich & Tremaine 1980; Lin & Papaloizou 1986c), but the debate about the exact migration rates of type II migration, relevant for gas giants in circumstellar discs, seems to be far from settled today (Kley et al. 2009; Hasegawa & Ida 2013; Robert et al. 2018; McNally et al. 2019; Scardoni et al. 2020) as those rates depend on a number of physical assumptions, particularly on the role of turbulent viscosity in circumstellar discs, which had to be recently completely re-evaluated in light of new measurements with ALMA (Pinte et al. 2016; Dullemond et al. 2018).

In light of those uncertainties concerning the initial formation locations of the giant (exo-)planets, during this thesis, work will be presented in an attempt to form giant planets on fixed orbits. This allows the study of the gas accretion process in a clean, numerical laboratory-like setting, without the disturbing effects of migration, which have been studied recently in Dürmann & Kley (2017) or grid noise that would be generated when an accreting planet migrates relative to the grid cells of the simulation domain. As the focus of this thesis is on the time of the active planet formation process in a circumstellar disc, a short account of how circumstellar discs form and what is known about them shall be given.

1.2 Star formation and the cluster environment

Modern astronomy can follow the star formation process, of which planet formation is a sideproduct, from its onset until the final planets emerge in circumstellar discs. Regions of the diffuse galactic medium (Bergin et al. 2004) can compactify themselves into giant, dark molecular clouds through the action of the galactic

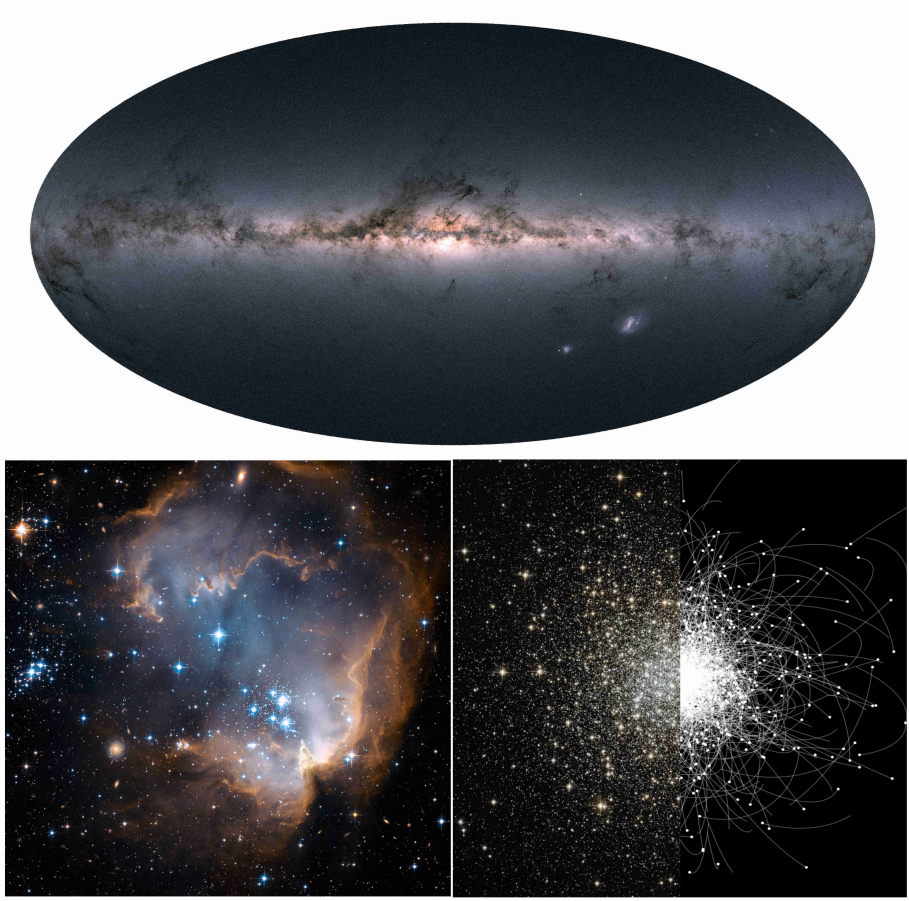

Figure 1.2: A zoom on star formation through space and time.
Top: Dust, as seen in dark molecular clouds throughout the local Milky Way, is a signpost of mass reservoirs for future star and planet formation. ©ESA/GAIA/DPAC
Bottom left: Planets are formed while their host stars reside in young clusters like NGC 602 (in the small magellanic cloud), a star cluster that just formed and is in the process of shedding its natal gas and dust mixture. ©Hubble/NASA/ESO.
Bottom right: Stellar clusters, as we see them in snapshots, are not static objects. Their constituent stars move on orbits (simulation and combined image of NGC 7006 ©Hubble/NASA/ESO/J. Dorval, reproduced with permission), which themselves change during the stars' residence time in the cluster. Circumstellar discs around those stars are blasted with strongly varying amounts of high-energy irradiation before they are ejected from the cluster.

tidal potential; those clouds then populate the galaxy and compactify further into cold clumps (Lada 2005), which self-gravitationally collapse (Stahler et al. 1981; Larson 2003) to form young stars and their associated circumstellar discs (van Dishoeck 2004). This process is depicted in some important snapshots in Figure 1.2.

The masses of giant molecular clouds allow for the simultaneous formation of entire groups of stars, called clusters. Most stars we see in the galaxy have been initially formed in clusters, then dynamically ejected from the same. The cluster environment is very dynamic. Stars orbit in the complex gravitational potential and can spend time at varying radii from the core of the cluster. As a few massive OB stars in the cluster can dominate the local radiative field, which can keep the circumstellar discs of lower-mass stars hot (Kölligan & Kuiper 2018; Ndugu et al. 2018) or even lead to lower dust masses in discs deep inside the cluster (Eisner et al. 2018). 3-D simulations indicate that dynamical infall events from the cluster onto circumstellar discs happen regularly (Padoan et al. 2014), consistent with the variability seen in protostars.

During the cluster formation process, as clouds fragment, some fragments can be of quite low mass, say only a few tens of Jupiter-masses. Those fragments form their own class of failed stars, brown dwarves, and for a time it was not clear whether the planet-mass objects discovered in the 1990's were not formed via such a process of cloud fragmentation. The discovery of the brown dwarf desert however (Grether & Lineweaver 2006), clearly set apart the low-mass tail of star formation and the high-mass end of planet formation. This was a definitive proof that planets are not direct products of the star formation process, but that of a secondary process, which is the formation of planets in circumstellar discs. Hence, this thesis considers planet formation in circumstellar discs. Furthermore it shall be mentioned that the term *circumstellar disc* therefore is often used as synonym to *protoplanetary disc*. The latter vocabulary is more popular nowadays and shall be used predominantly from now on. Of the two mainstream formation mechanisms of gas giants in protoplanetary discs, namely core-accretion (Mizuno et al. 1978) and disc-instabilities (Boss 2000), this thesis only considers the former.

The relatively late arrival of data which excluded planet formation scenarios by star-formation like processes, of course did not stop thinkers to conjecture about the actual physics of protoplanetary discs much earlier.

1.3 Gas giant birth environments I: Protoplanetary discs and a brief history of planet formation as science

Inspired by the flatness and coherent orbital angular momentum vectors of the solar system planets, Kant and Laplace already pursued ideas about the nature of a possible protosolar nebula in the 18th century. In modern vocabulary, Kant, in his work of 1755 essentially aimed to justify structure formation in the cosmos by differential gravitational settling in a multi-body, multi-species system. Some of those bodies would be of hypothetical, at that time yet undiscovered nature, which should allow them to be naturally slow, hence sink in the common gravitational potential of all the bodies and form the sun. The other parts making up the primordial mixture of matter and later the planets, would be the common elements as evidenced by chemists at that time. Laplace, towards the end of the 18th century, was less focused on the cosmos and more on the solar system, and employed the centrifugal force to stabilize an extended solar atmosphere and concentrate it into rings, which would form the planets. An important consequence of the Laplacian nebula would be a rapidly rotating sun as in this scenario no radial transport of angular momentum takes place.

While the ideas about the properties of the protosolar nebular were slowly developed over the subsequent centuries, it was in the 1950s-1970s that the theory of planet formation attained are more tractable and quantitative form. The works of Alfvén, Biermann, Goldreich, Safronov, Weidenschilling, Whipple and many others laid a theoretical foundation from which we deduct the majority of fundamental physics used today in the attempt to form and explain the existence of planets.

During the 1970s, it was due to deep space missions like Pioneer and Voyager that a more main-stream scientific interest erupted in the topic. This resulted in fruitful cross-pollination from the theory of cataclysmic binaries (Shakura & Sunyaev 1973), finally giving rise to a standard model of planet formation in circumstellar discs, under consideration of significant angular momentum transport.

It was however not until the 1980s that the first candidates for circumstellar nebulae were identified. Humanities first glimpes of those objects came in 1983/1984 when data by the IRAS satellite arrived in the form of spectral infrared excesses around nearby stars (the first ones being Vega, Formalhaut, β Pictoris and ϵ Eridani) (Aumann et al. 1984). The IRAS investigaton team was careful in their interpretation of this data and initially associated the infrared excesses with ejected circumstellar shells. Later in the same year, Smith & Terrile (1984) showed via the

detection of an optical counterpart of the infrared emission, that at least around the star β Pictoris those infrared excesses are associated with a flattened circumstellar dust disc. From the maximum orbital inclination of this disc, the possible range of dust masses and possible lifetimes of dust particles, they speculated that this debris disc might be associated with ongoing or successful planet formation processes. The association of those infrared-excess hosting stars with dust, and particular planet formation processes were later proven to be correct, with the discovery of the $\sim$30 Myr old exoplanet β Pictoris b by Lagrange et al. (2009) via direct imaging in the infrared, while planetary detections around the other three first infrared excess stars remain at large, or inconclusive up to this day.

While the initial discoveries of infrared excesses were limited to relatively isolated stars, it later became clear that most infrared excesses-bearing stars can be found in clusters, as opposed to field stars, which are generally understood to be cluster ejecta and hence older. The Spitzer and Herschel space telescopes helped to estimate the lifetimes of those infrared excess-hosting circumstellar discs as to be around 3-5 Myrs (Haisch et al. 2001; Mamajek 2009). Furthermore the occurrence rates of infrared excesses as well as exoplanets suggested a strong link between infrared excesses, circumstellar dust and planet formation (Najita & Kenyon 2014).

In the last decade, ALMA, the Atacama Large Millimeter Array, significantly increased the amount and quality of data available about protoplanetary discs to previously unknown levels. ALMA has allowed the astronomical community to spatially resolve known circumstellar discs at mm-wavelengths for the first time in significant numbers.

Many observed circumstellar discs possess a variety of interesting features like one-sided asymmetric blobs, rings, and spiral-like structures which appear in many ALMA images of resolved protoplanetary discs (Andrews et al. 2018) and accurate determinations of dust masses, the raw building blocks for planets, are now possible (Pascucci et al. 2016; Tychoniec et al. 2018; Ballering & Eisner 2019; Williams et al. 2019). Beyond that, the comparison of the measured dust masses with standard models led to a debate whether the relatively static model discs in classical planet formation theory need to be revised and what the role of infalling material from the cluster onto the CPD might be (Manara et al. 2018).

Accessing the gaseous component in protoplanetary discs, which in the end contributes to the majority of a gas giants mass, is much more difficult. Gas does not radiate at the cold temperatures and tenuous conditions in protoplanetary discs. Traditionally, also in this thesis, the dust-to-gas mass ratio, as determined in

the interstellar medium via Lyman α-absorption of stellar lines, is taken as $1/100$. It is then assumed that this dust-to-gas mass ratio remains constant in protoplanetary discs, until disc dispersal, grain settling, or other processes occur. With ALMA now, the dust-to-gas ratio becomes available also in those discs (Ansdell et al. 2016), and the determined values for the 1-3 Myr old K and M dwarves in the Lupus region can be both lower and higher than the canonical value of $1/100$, with a tendency towards the higher values. This indicates active gas depletion at those ages, consistent with the known dust disc lifetimes.

With all those results and more to come on the horizon, progress in understanding the planet formation process in the near future is inevitable. Particularly, a reassessment of gas accretion rates with updated simulation codes, such as performed in this thesis, is a timely endeavour.

It shall be now continued to review how the outcome of the planet formation processes is attempted to be constrained, through the search for young protoplanets in their natal discs.

1.4 Gas giant birth environments II: Features in protoplanetary discs and observed forming gas giants

In the endeavour to study protoplanets unspoiled by any processes other than planet formation itself, one cannot rely on the traditional exoplanet detection methods, such as the radial velocity and transit method. Those must necessarily fail in protoplanetary discs and therefore detection by direct imaging is a leading option. Giant planets with their expected high luminosities (Mordasini et al. 2017) and hence relative ease of detectability, are then the obvious targets to learn from.

The trouble locating protogiants however is that while old stars, which exist in large numbers, host planets which may be dynamically evolved. On the other end of the age scale, Class I and Class II (classical protoplanetary discs) often have large quantities of dust incorporated, making extinction of planetary signals a probable outcome, should planets form early. A small number of claimed, but then non-reproducible, detections of accreting protogiants in HD169142 (Reggiani et al. 2014), HD100546 (Quanz et al. 2015), LkCa15 (Sallum et al. 2015) may be explained by the effects of dust extinction (Szulágyi et al. 2019; Sanchis et al. 2020).

Furthermore, the possibility exists that some of the rings and spiral arms seen in ALMA images (Andrews et al. 2018) are associated with protoplanets. While

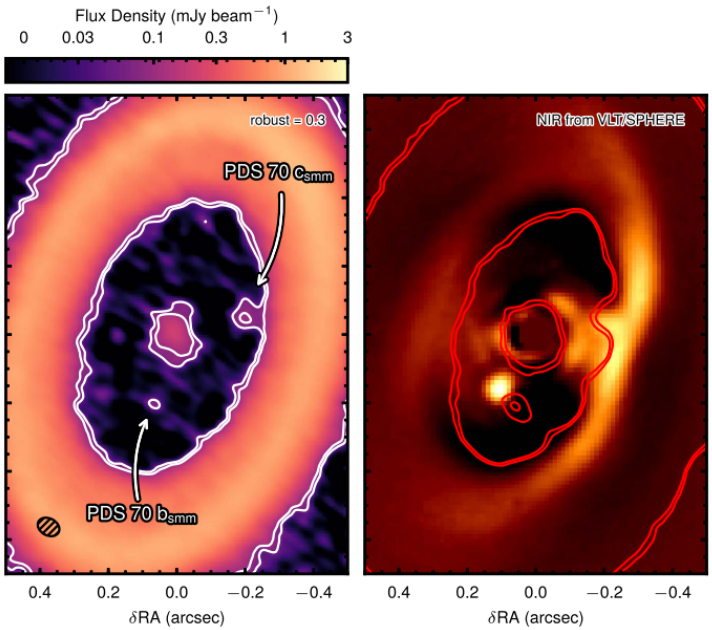

Figure 1.3: PDS 70, with companions b and c. Those planets are identified in the submm at 855 μm with ALMA (*Left*), and in the infrared Ks band (*Right*), and show additional accretion signatures in Hα (not shown). This evidence points to those companions being real accreting protoplanets. Red contours on the right are the same submm-signal as on the left, but with a different cleaning parameter. The offset between infrared and submm signals for PDS 70b is significant and not understood. ©AAS/Müller et al. (2018)/Isella et al. (2019), reproduced with permission.

so far only one protoplanet candidate exists to trigger such spirals in MWC 758 (Reggiani et al. 2018), some would assign a planet to each ring found so far based on statistical arguments (Nayakshin et al. 2019), while others would be less enthusiastic. Furthermore, at the low viscosities now known to persist in at least a fraction of protoplanetary discs, recent simulations have shown that multiple dust rings can be formed as results of the migration of low-mass planets (McNally et al. 2019).

A small number of gas giant planets have indirectly been detected via their kinematic distortions of gas line velocities (Teague et al. 2018). Those planets,

confusingly, seem to be of Jupiter-masses, but remain embedded in their protoplanetary discs, at odds with current thinking.

The only accreting, robust protoplanetary detections, which are revealed by their natal protoplanetary disc, are the planets orbiting the K7-type star PDS 70 at a 113 pc distance, see Figure 1.3. The protoplanets PDS 70b (Keppler et al. 2018) and PDS 70c (Haffert et al. 2019) survived multiple observation attempts (Müller et al. 2018; Mesa et al. 2019; Hashimoto et al. 2020), did not disappear, and share common source locations in the infrared, Hα and sub-mm fluxes. The latter is thought to be indicative of a circumplanetary disc around PDS 70c. The inferred age of PDS 70 is 5.4 ± 1.0 Myr (Müller et al. 2018), and the planet is therefore an ideal testbed for planet formation theory.

Together with the solar system giant planets, of which we know that they must have formed within a time of 3 Myr (Connelly et al. 2012), the known dust disk lifetimes in clusters (Mamajek 2009), and the gas lifetime in one (Ansdell et al. 2016), those ages formulate lower limits on the gas accretion rates of protoplanets of $10^{-4}\,\mathrm{m}_\oplus\,\mathrm{yr}^{-1}$, when forming a Jupiter-mass planet over this time.

In this thesis, work shall be presented addressing the self-consistent calculation of gas accretion rates onto protoplanetary cores, using a 3-D radiation hydrodynamical simulation code. After it was shown in Lambrechts & Lega (2017) that planets simulated with this code do not seem to accrete mass into its envelope, although radiation is lost from it, this was the first problem addressed in this work. The results include a thorough discussion of the pitfalls of simulating gas accretion with a radiation hydrodynamics code which uses the full viscous tensor and a Klahr & Kley (2006)-like planetary smoothing length. Beyond that, once gas accretion is measured, a semi-analytical understanding of the gas accretion rates found is reached, and the opacity dependency is characterized. Paper II presents results from the simulations of gas accretion rates at two different opacities for a wide range of planets, to emulate gas accretion which commences at Neptune-masses and terminates at Jupiter masses. Furthermore, it is shown under which conditions circumplanetary discs form, and their flow and structural variables are characterized. Paper III attempts to investigate the claim that PDS 70c contains mm-sized dust in its putative circumplanetary disc. With the hydrodynamic data from Paper II, detailed dust modeling and radiative transfer calculations are performed, it is found that mm-particle sizes are broadly consistent with the observations, assuming the claimed mass of the circumplanetary disc holds. Otherwise other particle sizes are consistent with the data as well.

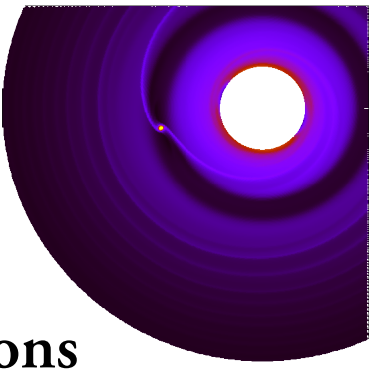

Chapter 2

Planet-disc interactions

In this short chapter important outcomes of interactions between forming protoplanets and their maternal discs are introduced. Those outcomes are spiral arms and planetary gaps, as can be seen in a simulation to the top right on this page. While being omnipresent in the simulations performed in this thesis, which necessitates their explanation, spiral arms and gaps also play a key role for the delivery of mass to protoplanets and its migration properties. However in this work, their role moves somewhat into the background, as this work focuses on the study of the physics of the protoplanetary envelope, which is neighbouring the spiral arms and gaps.

2.1 Spiral arms

Protoplanetary discs orbit their host star at near-Keplerian velocities $v_{\rm K}$ (Frank et al. 1985) featuring important velocity shear, as it is

$$v_K = \sqrt{\frac{GM_s}{r}} \tag{2.1}$$

where G is the gravitational constant and M_s is the mass of the central star and r the distance from the star. An observer could attempt to co-rotate with the disc, i.e. use a transformation into a rotating frame, as to be at rest with the disc at some radius $r_{\rm p}$. However, due to the nature of gravity which this flow must respond to, one will not find a radius at which the entire disc seems to be at rest. Furthermore, due to this shear there exist radii neighbouring $r_{\rm p}$, termed $r_{\rm L}$, in the disc at which

an observer at $r_{\rm p}$ will see neighbouring gas passing by every k orbits. As gas further away from $r_{\rm p}$ has a higher relative velocity to it, it will see the same gas parcels move by more often, than gas parcels close to it. This effect of 'seeing' a gas parcels passing by will become very important when $r_{\rm L}$ corresponds to distances from $r_{\rm p}$ where the seeing happens regularly, i.e. when k is an integer number. The locations $r_{\rm L}$ are then called Lindblad-resonances (Goldreich & Tremaine 1978) and are located in the disc at radii (Armitage 2010)

$$r_{\rm L} = \left(1 \pm \frac{1}{k}\right)^{2/3} r_{\rm P}. \tag{2.2}$$

Note how this discussion involves no planets so far, only the gas dynamics around the star. When we add a planet into the argument, this planet can perturb all those resonances, in principle. One can then think of the gas parcels passing the planet as strings, being periodically plucked by the planet. In general the planet will not be able reach all those resonant locations initially. The 'reach' of a planet can be calculated as its radius of dominating gravitational influence, called the Hill-radius, which for a planet of mass $m_{\rm P}$ is found as (Murray & Dermott 2000)

$$r_{\rm H} \equiv \left(\frac{m_{\rm p}}{3M_{\rm s}}\right)^{1/3} \tag{2.3}$$

The more massive the planet gets, the larger $r_{\rm H}$ becomes. The low-order resonances, which according to Equation 2.2 and the preceding rationale, are located farther away from the planet than the high-order resonances. Hence, as the planet grows in mass, in general its reach will incorporate stronger and more resonances, which leads to a nonlinear growth in the strength of the gravitational perturbations which this planet exhibits on the global circumstellar gas flow. Finally, the response of the disc gas must be discussed. Every perturbed location in the circumstellar disc will send out sound waves as a response to the perturbation (Lin & Papaloizou 1986b). As there are many such perturbed locations, which are regularly perturbed, they all send out sound waves with their local sound speeds c_s, which overlap and form a common sound-propagation surface. This surface will propagate through the disc and is additionally advected along with the gas velocities.

Another factor playing a decisive role in the physics of circumplanetary discs is that they are supersonic on a local scale of the disc-scale height H, i.e.

$$\frac{c_s}{v_K} \approx \frac{H}{r} \tag{2.4}$$

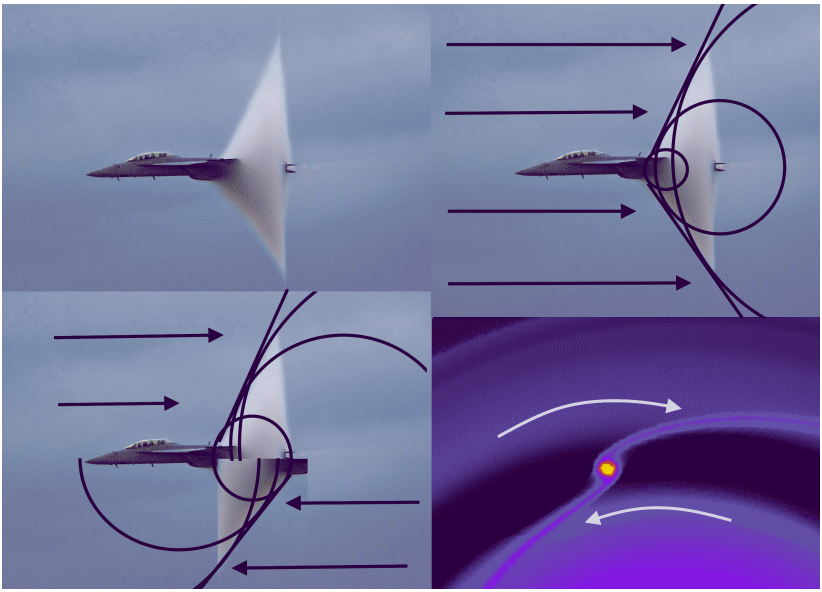

Figure 2.1: **Top Left:** The formation of spiral arms in a circumstellar disc can be discussed akin to a periodically returning supersonic jet, with its Mach cone embedded in a strong shear flow. **Top right:** In the reference frame of the jet, gas is flowing at it from the front. Overlapping sound-waves add up to a resonant surface - the Mach shock. **Bottom Left:** Now we embedded the Jet in a strong vertical shear flow, similar to the global flow in a circumstellar disc. In the jet rest-frame, the flow comes from both sides and hence, the Mach shock is asymmetric. **Bottom right:** In a circumstellar disc the situation is more complex, as the perturber returns periodically. This gives rise to multiple spiral shocks, launched from locations that are resonant with the planetary perturbation. ©Realbigtaco via Wikipedia, CC Licence 3.0

and typical values of H/r are a few percent in radiative discs (Bitsch et al. 2013). Therefore the common sound surface, launched by all resonances, will steepen into a shock surface, which gives birth to the structure commonly referred to as the planetary spiral arm.

A flawed, but graphic, and maybe more familiar situation to this process is offered here as analogy to a Mach-cone in Figure 2.1 via the travelling of a supersonic jet through the terrestrial atmosphere. The role of the perturbing gravity is now taken over by the physical incompressibility of the jet, which drives sound

waves into the incoming gas. Due to the lack of a periodically recurring medium, there is only one resonant location. If one would somehow reverse the direction of the bottom flow and keep it supersonic, a superficially analogous situation to a planet in a circumplanetary disc could be created.

2.2 Gaps

As a planet grows in mass, via processes that will be discussed later, its associated spiral arms grow in shock strength and overdensity relative to the surrounding disc. At a certain point perturbations by the spiral arms become strong enough to eject mass from the initial gas trajectories, and their influence on the global flow becomes noticeable. The distortions caused by the spiral arms are such that they expel gas radially away from the planet. Once the gas attains some distance to the planet, viscous diffusion and pressure gradients act to restore the initial trajectory of the gas. Should those forces prove to be insufficient, a planetary gap will open, as illustrated in Fig. 2.2 and analysed in a large body of works since Goldreich & Tremaine (1980).

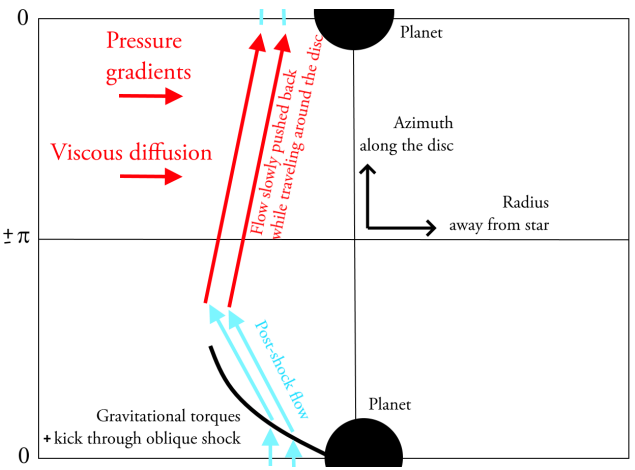

Figure 2.2: A sketch of gap formation, motivated by Lin & Papaloizou (1986a). The strength and attack angle of the shock depends on the ambient disc conditions, particularly the temperature, which sets the local speed of sound. The action of the shock and gravitational torques kicks gas out of the orbital path of the planet. When viscous and pressure gradients are unable to restore sufficient mass flux into the planetary orbit, a gap forms.

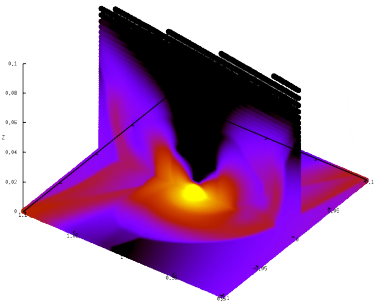

Chapter 3

The core accretion problem: All eyes on the envelope

In this chapter the crucial ingredients to understand current ideas about the formation of gas giants in the core accretion paradigm are presented. Subsequently, simple envelope solutions are discussed and contrasted with the mode of quasi-hydrostatic gas accretion found in numerical results obtained in this thesis. Finally, the numerical results are covered, starting from Neptune-like planets at 20 $m_\oplus$, up until the protoplanets have reached Jupiter masses of 320 $m_\oplus$. In relation to the last chapter, the Neptunian-like planets are traditionally thought to be in the mass regime which forms spiral arms in circumplanetary discs, while gaps are formed at larger masses (Goldreich & Tremaine 1980; Crida et al. 2006).

3.1 Elements of classical core accretion theory

The core-accretion scenario (Mizuno et al. 1978), or core-nucleated instability, is one of the classical pathways to form giant planets and the focus of this work. This is a bottom-up scenario, i.e. a scenario that forms small scaled solids first, for those to grow successively larger. The core grows by means of collisions of planetesimals (Pollack et al. 1996) or by the accretion of pebbles onto a seed planetesimal or seed protoplanet (Lambrechts & Johansen 2012; Morbidelli et al. 2015). The formation of the smaller planetesimals again is possible via the mechanism of the streaming instability (Johansen et al. 2007; Simon et al. 2016), or fluffy dust growth (Kataoka et al. 2013), but planetesimal formation shall not be further discussed in this thesis.

Grace to the efforts and results from the Juno mission, which have recently been published, and their comparison with new interior structure models of Jupiter (Wahl et al. 2017), it seems certain that Jupiter's core is consistent with the mass required from core accretion models (Mizuno 1980; Bodenheimer & Pollack 1986; Pollack et al. 1996; Piso & Youdin 2014) which can be built within standard disc theory assumptions. However, those new results also indicate an important heavy element pollution in the deep jovian atmosphere. Re-updated structural models of Jupiter (Debras & Chabrier 2019) seem to be able to fit its current mass, radius, rotation and heavy element pollution, where the latter, as indicated initially by measurements via the Galileo probe (Wong et al. 2004), was previously considered a problem, which now seems a natural outcome of the core pollution scenario. Additionally, assuming similar pollution models for the deep atmospheres of the ice giant Uranus, it seems also to be possible to explain its luminosity (Vazan & Helled 2020; Helled et al. 2020), previously thought anomalously low for decades (Hanel et al. 1986; Lunine 1993).

One possible reason for the solid pollution of the deep atmosphere is given by results from molecular dynamics simulations showing that the ice and rock compounds presumably forming the core should be thermodynamically unstable, i.e. soluble in the high-pressure H/He mixture in the interiors of gas giant planets (Wilson & Militzer 2012; Wahl et al. 2013) and therefore lead to an 'eroded core' and a heavy-element polluted planetary interior. The heavy element content of Jupiters atmosphere seems to be alternatively possible to explain via a late veneer of impactors (Liu et al. 2019) during their formation, which would simultaneously be a plausible model for the Uranian axial tilt.

However, as the interpretation of those recent results, particularly the timing of the significant solid pollution in the Jovian deep atmosphere is unclear at the moment, the work in this thesis considers a conservative approach to the formation of the giant planetary core, and considers it to be already in place with all its mass, when launching simulations.

In the classical scenario of giant planet formation, during the build-up of the core, growth of the gaseous components of the planet sets in, triggered by the increasing gravitational attraction of the core. As consequence a tenuous, extremely extended atmosphere forms, which remains connected to the parental protoplanetary disc during a significant fraction of the entire growth process of the protoplanet, and hence receives a special designation, as *the envelope*.

The ongoing accretion of solids onto the core releases enormous amounts of energy. This energy release can either happen via friction with the envelope, latent

heat of sublimation or mechanically, when large planetesimals hit the core. And although the protoplanetary envelope will be cooling to some degree, this concurrent accretion of solids and gas (Pollack et al. 1996) can delay the envelope from growing in mass for a significant time.

Once the solid accretion ceases, either through the depletion of a local planetesimal feeding zone, or by reaching its pebble isolation mass (Lambrechts et al. 2014), the opacity of the nebula may allow it to cool and compactify (Hubickyj et al. 2005). A potentially very long phase of hydrostatic envelope growth follows, which is depicted for the solid ($M_{\rm Z}$) and gaseous ($M_{\rm XY}$) components of the protoplanet in the red curves in Figure 3.1, taken from Movshovitz et al. (2010). During this phase still the small solids, commonly referred to as dust, hold a key power over the envelope, as they are controlling the cooling time of the gas. Once dust grows, the cooling time decreases[1], as shown in the blue and black curves in Figure 3.1. In that particular work, the dust growth is self-consistently controlled by the local solid mass density, i.e. a higher solid mass that allows dust to grow quicker, which allows the gas to cool more efficiently. In total this process can shorten the long, hydrostatic growth phase of the envelope significantly.

Once the gaseous mass manages to double the initial total mass of the planet, one speaks of the gas having reached *crossover mass*. This is a significant moment, as now the first mass doubling is successfully finished. From here on, the higher gravity of the total planet mass conspires with the increasing luminosity to let the planet reach *runaway gas accretion* (Mizuno et al. 1978), which is the peak in luminosity and mass seen in Figure 3.1. The luminosity is the formal equivalent of the aforementioned cooling capability of the envelope. In 1-D static models this is usually the moment in which the computation has to finish, although with hydrodynamical models in 1-D (Wuchterl 1991) and 3-D (Ayliffe & Bate 2012) it is possible to probe the planetary evolution beyond the runaway gas accretional collapse of its envelope.

[1]The cooling time of a gaseous envelope in the diffusive regime is given by the opacity of its dust content. This is due to two reasons. First of all, dust and gas are usually in thermodynamical equilibrium w.r.t each other and hence their internal energies are coupled efficiently. Secondly, when neglecting scattering effects, the opacity of dust is given by its total geometrical dust cross section. Let a number N of dust particles of size r, representing a constant total mass $M = N \times \rho \times 4/3\pi r^3$ with solid density ρ and its total blocking surface $A = N \times \pi \times r^2$ grow. Once one expresses A with only constants and r, it is seen that the total cross-section decreases as the dust grows, and it is $A \propto \rho \times M/r$.

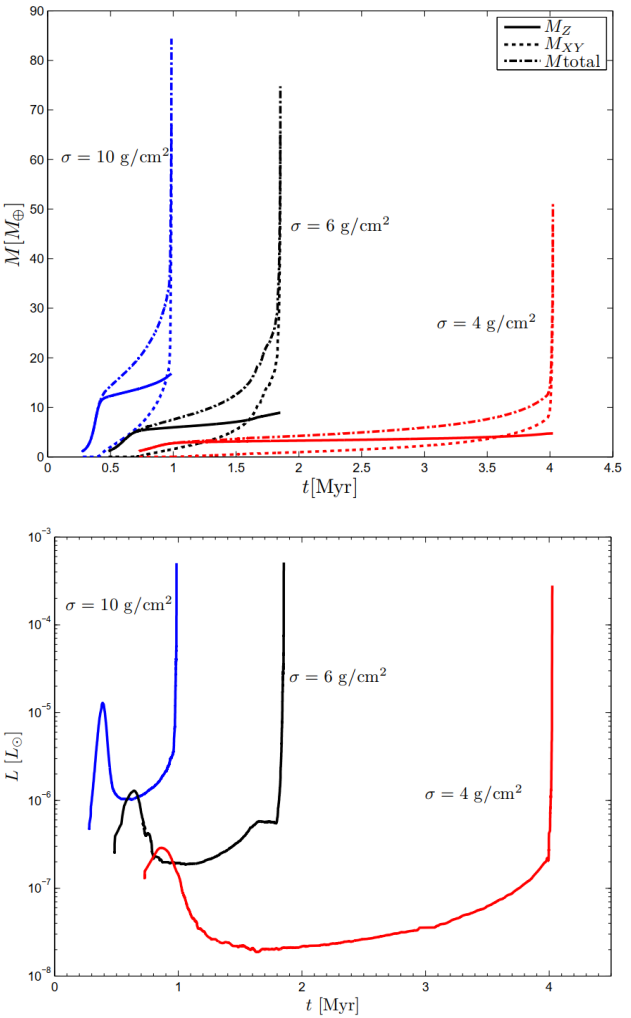

Figure 3.1: 1-D Simulations of the growth of gas giants by ©Movshovitz et al. (2010) (reprinted with permission), according to a classical recipe by Pollack et al. (1996). The recipe incorporated the growth of a solid core (M_Z) through accretion of planetesimals, which was stunted after ∼0.5 Myrs. A long phase of hydrostatic gas accretion follows, when the gas mass in the planetary envelope (M_{XY}) slowly increases, particularly notable for the low-surface density models (red curves). Their work linked the surface density σ in the protosolar nebula to the coagulation timescale of the dust, which again controls the opacity. With this they were able to show self-consistently how to shorten the long, hydrostatic accretion phase significantly.

Following this summary, it shall be outlined how luminosities can be computed, generally and in this thesis. Assuming an object that is 1-D spherically symmetric and possesses a surface, one can compute the luminosity simply as

$$L = 4\pi r_{\tau=1}^2 \sigma T_{\text{eff}}^4 \tag{3.1}$$

with T_{eff} being the temperature at radius $r_{\tau=1}$, and σ the Stefan-Boltzmann constant. The radius $r_{\tau=1}$ is the radius which one would interpret as the surface, or photosphere, and it can be found the as radius at which the *optical depth*, defined as

$$\tau \equiv \int_{x_0}^{x_1} dx' \rho(x') \kappa(x') \tag{3.2}$$

reaches unity[2], with the envelope density structure $\rho(x)$ and the opacity of the dust/gas mixture $\kappa(x)$. This radius is classically understood as a photospheric radius, or just *the* radius of a star or planet[3].

When choosing $x_0 = +\infty$ and $x_1 = r_{\tau=1}$, then setting $\tau = 1$, this gives an implicit equation to find the photospheric radius $r_{\tau=1}$, which can be solved analytically in special cases or must be found numerically for complex structures $\rho(x)$ and $\kappa(x)$. A discussion of the wavelength and compositional dependence of $\kappa(x)$ is omitted for now and this variable is treated as one constant, grey value for the sake of this introduction.

With those concepts established, all ingredients are set in place in order to understand the behaviour of the luminosity and mass accretion curves of growing protogiant planets. The loss of internal energy of the gas, mediated via the escaping photon luminosity, is directly coupled to the contraction and subsequent accretion of more gas into the protoplanetary envelope. During the hydrostatic phase it can be established via timescale arguments that

$$L = \frac{G M_{\text{planet}} \dot{M}_{\text{gas}}}{r_{\text{core}}} \tag{3.3}$$

[2]Formally it is $\tau = 2/3$ which gives the photospheric radius (Mihalas & Mihalas 1984), but we use $\tau = 1$ throughout this thesis due to its superior beauty, educational value, and the radius errors from this small correction are negligible in all cases.

[3]Another convention for giant planets often cites the radius at which the pressure reaches 1 bar as *the* radius. This measure of radius is usually roughly compatible with the $r_{\tau=1}$ measure up to an atmospheric scale height, as most gaseous opacity sources, in the absence of clouds, will broaden their banded line contributions into a nearly totally opaque absorption continuum between pressures of 0.1-1 bar due to significant pressure broadening. This is obviously only a rule of thumb, as Earths atmosphere is only semi-transparent at 1 bar pressure.

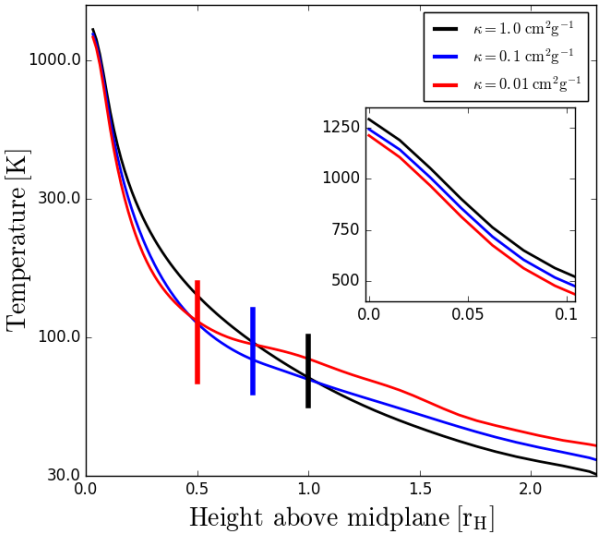

Figure 3.2: Example vertical temperature profiles in protoplanetary envelopes resulting from a simulation run after 10 orbits time with a 90 $m_\oplus$ protoplanet. This plot emphasizes the effect of increasing the optical depth in the envelope via a change in opacity. $\tau = 1$-transitions are marked with vertical lines for each simulation. All three simulations are initialized by compactifying the same gas mass into the gravitational potential -$GM/r_{\rm core}$ and therefore start out with identical adiabatic temperature profiles. After 10 orbits the vertical temperature profiles have dramatically evolved and found a new equilibrium. A low opacity helps to significantly decrease the overall temperature profile, and particularly the central temperature with time. Furthermore, it becomes clear how a larger $T_{\rm eff}$ leads to a smaller $T_{\rm central}$ (shown in the inset). The ongoing quasi-hydrostatic accretion process can qualitatively be thought of as slow change from the red to the blue to the black line, as the optical depth increases.

with the gravitational constant G, $M_{\rm planet}$ the total mass of the planet, $\dot{M}_{\rm gas}$ the gas accretion rate of the planet and $r_{\rm core}$ the radius of the gravitational potential into which gas is accreted. Therefore, if the luminosity can be predicted, or post-predicted, then a tool to understand the accretion rates seen in Figure 3.1, as well as those found in the simulations with FARGOCA in this thesis, based on density-temperature structures only, has been created.

In the core accretion scenarios, the envelope luminosity decreases at first, be-

cause as the envelope is accreting gas, its optical depth increases. It is possible to see this, when using the fundamental relation between the temperature profile in radiative solutions and the effective temperature (Mihalas & Mihalas 1984)[4],

$$T^4 = \frac{3}{4}\left(\tau + \frac{2}{3}\right) T_{\rm eff}^4 \tag{3.4}$$

reversing this for $T_{\rm eff}^4$, using $\tau \gg 2/3$, and plugging this into Equation 3.1 yields

$$L \approx \frac{4\pi r_{\tau=1}\, T^4}{\rho\kappa}. \tag{3.5}$$

where now T can be e.g. the central temperature. The initial accretion process is quasi-hydrostatic, hence it can be safely assumed that a variation of r on occurs on typical scale heights of $\sim$100s of km, while the density will vary exponentially on those scales.

Hence, during quasi-hydrostatic gas accretion, the luminosity will decrease with time as a consequence of increased optical depth of the envelope. When the luminosity prediction from structural considerations, Equation 3.5, is combined with the luminosity-accretion rate relation, Equation 3.3, it is furthermore possible to qualitatively see that $\dot{M}_{\rm gas} \propto 1/M_{\rm atmo}$, hence the accretion rate slows down with time as well.

This analysis is furthermore important, as it explains the temporal evolution and opacity-dependent behaviour of the gas accretion rates seen in Paper I. For the latter, we show an illustrative example in Figure 3.2. It shall be noted, that a 1-D optical depth has been only used for the sake of the argument here, as a luminosity computed from a 1-D optical depth in general does not explain the 3-D data well. In order for luminosity and accretion rates to match, the full 3-D structure of the $\tau = 1$-surface has to be taken into account.

When self-gravity is included, this serves as a game-changer. The contraction from self-gravitation is able to store the accreted atmospheric mass inwards of $r_{\tau=1}$, instead of covering it. This moves $r_{\tau=1}$ inwards to hotter temperatures, increasing the luminosity. Then, the more the planet accretes, the larger $T_{\rm eff}$ grows, the more it can accrete again. This principle lies at the basis of the process of runaway gas accretion, mentioned above, and it is already possible to see its humble

[4]More detailed analyses exist, taking into account the effects of optically thin radiation and scattering (Hubeny 1990), but the formula cited above serves the point.

beginnings in Fig. 3.1 at fairly early stages, whenever the planetary luminosity increases with time.

Now the physical framework shall be introduced that was used to solve for the envelope structures of planets and it will be explained how the approach used throughout this thesis differs from the classical framework that was just discussed.

3.2 FARGOCA, the snapshot approach and the equations of radiation hydrodynamics

The computations presented in this thesis are able to self-consistently model the dependence of the gas accretion process onto protoplanetary cores in a global 3-D environment, without the need for sink-cells. As the computational restrictions on the number of orbits the simulations are able to run in high resolution are quite severe, it is only possible to follow gas accretion curves like the ones seen in Fig. 3.1 in snapshots. Furthermore, as the models presented here do not include self-gravity, all planetary envelopes remain in a state of quasi-static contraction and do not reach formal runaway gas accretion, although equivalently high accretion rates occur in this setting. To this end, several sets of opacities were chosen, namely constant values of $0.01 - 1.0\,\mathrm{cm^2\,g^{-1}}$, the tables given by Bell & Lin (1994), and the combined tables by Semenov et al. (2003) & Malygin et al. (2014).

The physical parameters are the viscosity, which is a constant throughout this work with $\nu = 10^{-15}\,\mathrm{cm^2\,s^{-1}}$, and corresponds roughly to an $\alpha \approx 10^{-2}$, a constant adiabatic index $\gamma = 1.4$, several planet masses ranging from 20 $\mathrm{m_\oplus}$ to 360 $\mathrm{m_\oplus}$, and an appropriate set of initial conditions pertaining to those masses, in order to measure their accretion rates and characterize their envelope structures.

The tool of choice to simulate this process is the code FARGOCA (Bitsch et al. 2014; Lega et al. 2014). FARGOCA solves the equations of a radiating hydrodynamic gas with an ideal and adiabatic equation of state in three spatial dimensions. Because the planets which were was investigated were embedded in global circumstellar discs, and the nature of those circumstellar discs is such that they possess significant velocity shear, traditionally it is the inner disc edge which leads to significant computational speed limits.

Therefore, the advection problem in the azimuthal direction, which is the direction along the planetary orbit (see also Figure 3.3) is solved via employing the FARGO-algorithm (Masset 2000). The other half of the code acronym is explained through the main location of development, which is the OCA (Observatoire du Côte d'Azur in Nice, France). Historically, this code was developed

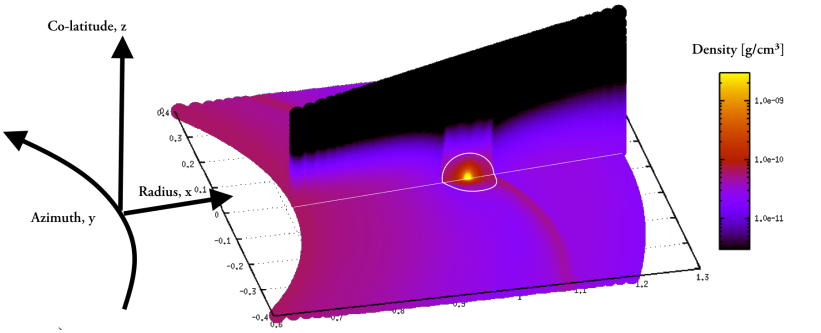

Figure 3.3: Density structures both in the midplane ($z = 0$) and in a vertical cut through the planet ($y = 0$), for the envelope of a protoplanet slightly more massive than Neptune, 20 $\mathrm{m}_\oplus$ for a low envelope opacity of $\kappa = 0.01\,\mathrm{cm}^2\,\mathrm{g}^{-1}$. The approximate Hill-sphere of radius r_H is marked with projected white circles. Evident is the global embedding in the disc and the spiral arm, which the planet is triggering in the flow. Vocabulary for naming the cardinal directions are included. This is in the widest sense an envelope: The planetary atmosphere is far extended into the Hill-sphere of the planet, and it is evident how the disc material still encroaches close to it. At this phase, one also speaks of an embedded planet.

separately from FARGO3D (Benítez-Llambay & Masset 2016) with the third dimension and radiation transport in mind. For more details on the equations the reader is referred to Paper I. For readers interested in the numerical details behind this and aspects of code execution for hydrodynamic hybrid simulation code as well as the grid structures used in this thesis, a reference to Chapter 5 is given here as well.

No hyperbolic differential equation can be solved without boundary and initial conditions. Every individual planet mass during the snapshot procedures was run in several steps consecutive steps, each providing boundary and initial conditions for the next, in order to speed up the physics of radiative disc equilibrium, gap formation and accretion. Details on those processes can also be found in Paper I. This methodology is, for the sake of readability of this introduction, repeated in Chapter 5.

Finally, the code solves for the zeroth moment of the radiation field with the flux-limited diffusion approach (Levermore & Pomraning 1981) as closure relation. This makes it possible to accrete gas permanently through radiating away the compressional heat and viscous entropy associated with gas inflow into the

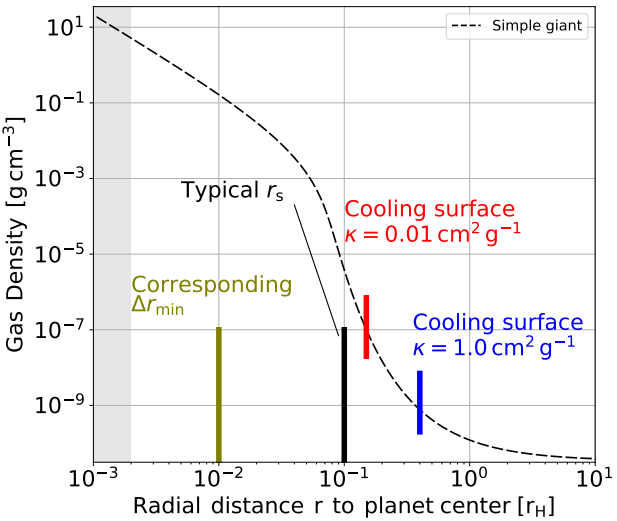

Figure 3.4: Summary of the most important physical scales in the protoplanetary envelopes in this thesis, particularly in relation to Fig. 3.3. $\tau = 1$-surfaces are marked for two analytical test models which differ in opacities by $\times 100$. A typical value of the smoothing length, as well as the corresponding minimum cell size according to our resolution criterion. A typical planetary radius is marked as grey area to the left. At $r/r_\mathrm{H} > 1$ is the domain of the circumstellar disc.

envelope.

Initially, however this accretion process did simply not occur, although the envelope was cooling, and the reason for this was unknown. Results from the investigation into this shall now be briefly stated, as well as the resolution of this problem. In FARGOCA, the planet is represented by a smoothed gravitational potential Φ'_p after Klahr & Kley (2006),

$$\Phi'_\mathrm{p} = -GM_\mathrm{p}\left[\frac{r^3}{r_s^4} - 2\frac{r^2}{r_s^3} + \frac{2}{r_s}\right], \tag{3.6}$$

with a characteristic size r_s, called the *smoothing length*, and planetocentric radius r. Outside of r_s the usual potential $\Phi_\mathrm{p} = -GM_\mathrm{P}/r$ is given. One of the key results from Paper I was that the scale r_s needs to be resolved with 10 grid cells, in order for gas accretion to occur and attain numerically convergent values. For

a reference of scales, the deepest smoothing length which was used and properly resolved in this thesis, in the envelope of a Jupiter-mass planet in relation to other relevant length scales, is plotted in Figure 3.4.

A symptom related to the non-accretion problem, was found to be the overestimation of the viscous work of the infalling gas into the smoothing length region. For a well-resolved simulation the ratio of total compressional to viscous work was about 0.1. Underresolving the smoothing length led to this ratio becoming unity. This led to a cessation of accretion.

The deeper connection between the cessation of accretion and the overestimation of viscous work is now as follows. The gas falling into the planetary potential will at first be adiabatically compressed, particularly in the deep parts of the envelope, where radiative timescales are long. Hence the gas will have the temperature corresponding to its initial adiabat (which shall be expanded on in the next section). Thermodynamically, this is a maximum temperature. There is no density structure that fulfills the hydrostatic equation and is hotter. Increasing the temperature further, beyond this limit through any means, will result in a thermodynamically unstable envelope, and hence an outflow will be triggered. In a way this would correspond to an anti-Mizuno et al. (1978) solution. When underresolving the envelope, and viscous work would become important, this overestimated viscous work would play the exact role of tipping the energetic balance over the adiabatic limit.

A rationale for why the number of well-resolved cells is 10, and not say, 20 or 133, shall also be given here. With the given form of $\Phi'_{\rm p}$ the infalling gas is not actually force-free, after it passes inwards of $r_{\rm s}$. The maximum of the radial acceleration that $\Phi_{\rm p}$ imparts on the gas can trivially be confirmed to be located at $r = \frac{2}{3} r_{\rm s}$, i.e. inside the smoothing length, which comes from the fact that the smoothed and actual potential are connected in their 1st and 2nd derivative at r_s. When computing the resulting forces $F = -\partial \Phi_{\rm p}/\partial r$ it is $|F(\frac{2}{3}\, r_{\rm s})'| < |F(\frac{2}{3}\, r_{\rm s})|$, so the acceleration inside the smoothing length is not unphysically large, but it is also nonzero. Hence, the criterion of 10 cells per $r_{\rm s}$ is actually corresponding to 6 cells per innermost, slowly relaxing envelope.

Solving this puzzle occupied the author of this work for a significant fraction of his early PhD time, and it has, amongst other findings been published in Paper I. Finally, armed with this knowledge, simulations of gas accretion proper were begun.

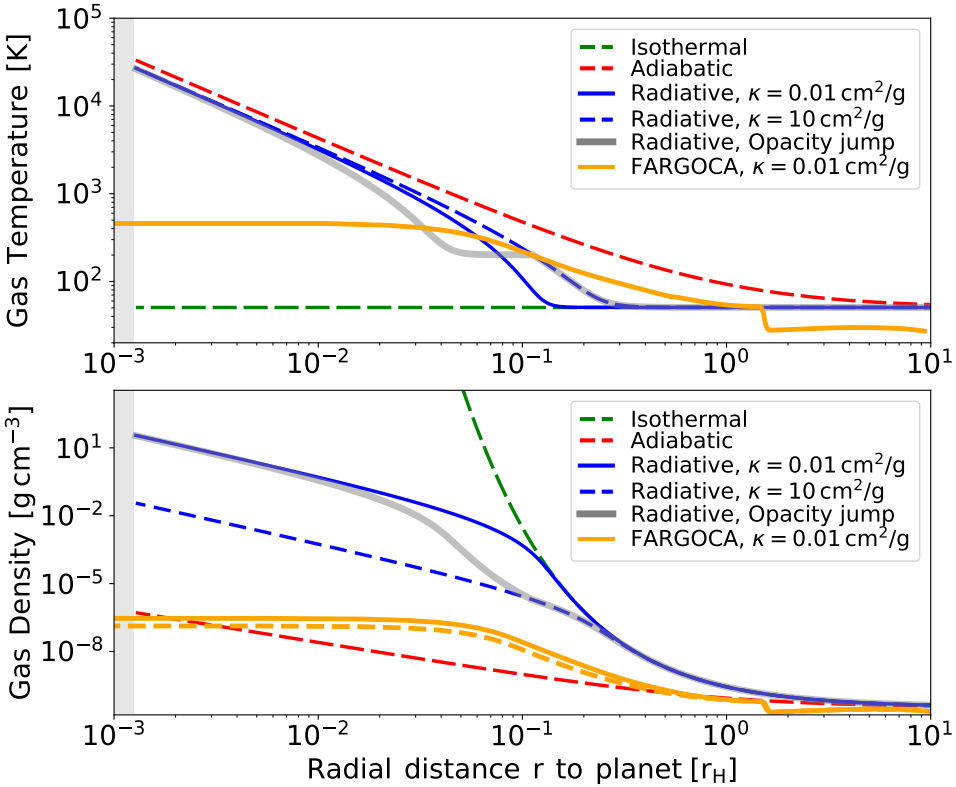

Figure 3.5: Envelope structures for a 20 $m_\oplus$ planetary core, for different types of energy treatment. Models are 1D-spherically symmmetric and hydrostatic, except FARGOCA. The 1D models are solutions of the classical stellar structure equations starting from the disc boundary conditions at $r = 100\, r_\mathrm{H}$ inwards. The full 3D hydrodynamic solution with FARGOCA (dashed orange line and solid orange line 5 orbits later) is well-resolved down to $r = 0.1\, r_\mathrm{H}$, therefore the cut-off in values occurs. This solution shows elements of all those solutions, with important differences: As the 3-D envelope radiates energy partly into the disc, partly into space, the envelope contracts adiabatically and new gas is accreted from the disc. This has the net effect of keeping the temperature gradient in the midplane adiabatic, imparting enormous vertical luminosities, while the density profile builds up mass, preferentially in the interior of the envelope.

3.3 Static envelope structures and the onset of gas accretion in FARGOCA

This section shall briefly discuss the most popular approximations which solve the density-temperature structures in the envelopes of embedded planets. A fundamental property of any of those structures is that they have to fulfil the hydrostatic equation, but the pressure gradients needed to balance gravity can be yielded by various combinations of density and temperature.

Example solutions of the stellar structure equations allow to compare those different means of energy treatment to the full 3-D radiative hydrodynamic solution obtained with FARGOCA during the ongoing early gas accretion phase, which are presented in Fig. 3.5. This, on one hand, will familiarize the reader with the typical expectations due to those approximations in the research literature, but also provides details on the global quasi-hydrostatic 3-D accretion process, which are otherwise not accessible. For this example, a planet of 20 $\mathrm{m}_\oplus$ is used.

The simplest approximation is the isothermal approximation, assuming $P = c_\mathrm{s}^2 \rho$, where c_s^2 is the square of the local sound speed, representing the temperature and mean molecular mass. As the name suggests, this assumes a constant local temperature throughout the simulation domain at constant composition. As a consequence, the necessary pressure gradients that are needed to satisfy the hydrostatic equation can only be reached via enormous increases in density. More precisely, isothermal envelopes feature exponential density structures in 1-D, and similar behaviour is seen in 3-D simulations of protoplanetary envelopes (Tanigawa et al. 2012; D'Angelo & Podolak 2015; Béthune 2019). While isothermal regions in reality certainly exist anywhere where $t_\mathrm{cool} \ll t_\mathrm{heat}$, including the far outer regions of radiative envelopes, the application of this approximation to deep, optically thick envelopes and measurements of accretion rates is highly doubtful.

The framework which traditionally covers the other end of the cooling time spectrum, $t_\mathrm{cool} \to \infty$, is the adiabatic approximation. This framework solves additionally for the temperature given by the adiabatic and ideal equations of state $P = (\gamma - 1) e_\mathrm{int}$ and $e_\mathrm{int} = c_\mathrm{V} \rho T$. However, in this framework any temperature variations are results of adiabatic compression or expansion and hence dictated by the absolute conservation of entropy. Volumes of differing entropy can only be connected via shocks in the adiabatic approximation.

When coupling the equation for e_int to a radiative energy equation, one can access all values of t_cool, which is proportional to the previously introduced optical depth, $t_\mathrm{cool} \propto 1/\tau \propto 1/\rho\kappa$. As adiabatic and isothermal approximations

are often quoted as bracketing either end of the cooling spectrum and hence realistic density-temperature structures, it becomes evident from Fig. 3.5 that this bracketing allows for an enormous range in structures. By taking the radiative approximation, and considering a range of sensible opacities κ one can narrow down this bracketing-argument.

This range of opacities is usually considered to be bracketed at the high end through opacities given by the properties of the dust in the interstellar medium (Ossenkopf & Henning 1994) as $\kappa = 10\,\mathrm{cm^2\,g^{-1}}$. Through the growth of dust this value can decrease down to $\kappa = 0.01 - 0.001\,\mathrm{cm^2\,g^{-1}}$ in the envelopes of giant planets (Mordasini et al. 2014). As is obvious from Fig. 3.5 (solid blue and dashed blue curves), this narrows the possible range of density structures quite severely. Additionally, opacities are in reality not constant throughout planetary envelopes. Opacity discontinuities occur when strong opacity sources, such as water ice, various minerals or carbon-bearing species sublimate and momentarily increase the transparency of the gas/dust mixture. This can trigger a very low, quasi-isothermal temperature gradient and the associated high density gradients, for a limited range in radii. As illustrative example an unrealistically high opacity discontinuity set at $T = 200$ K, is featured between the minimum and maximum values of opacities, in the grey curve. This guides the expectations for more realistic opacity law which have been used in Paper I.

Finally, one can observe how the 3-D envelope with the full energy treatment behaves, for a low opacity case of $\kappa = 0.01\,\mathrm{cm^2\,g^{-1}}$. The corresponding profiles are presented in the midplane (the x-y plane, or $z = 0$-plane), as shown in Fig. 3.5 in the orange curve. There, it can be noted how the mass in the envelope increases slowly over the course of 5 orbits (dashed orange to solid orange curve). The density structure departs from its post-spiral arm shock adiabat and shows a gradient commensurable with a radiative solution, as would be expected due to the cooling of the gas. However, when inspecting the temperature profile of the full solution it is obvious that the solution is an adiabatic profile.

This is a fundamental feature of the 3-D solutions in this work, which 1-D models necessarily fail to reproduce: While the vertical direction cools off and presents a radiative profile, the midplane contracts and accretes material, presenting itself at adiabatic temperatures. In the light of the preceding discussion on luminosities, this showcases why 3-D accretion rates can be higher than their 1-D counterparts. The adiabatically contracting midplane keeps the entire envelope hot, leading to large T_{eff} in the vertical hence high luminosities and accretion rates. This could explain why the measured accretion rates are even above those of Ayliffe

& Bate (2009b), as published in Paper II.

Additionally, the simulations presented in this thesis included a 20 $\mathrm{m}_\oplus$ planet with a high opacity envelope of $\kappa = 1.0\,\mathrm{cm}^2\,\mathrm{g}^{-1}$. There, both density and temperature profiles were much closer to adiabatic in the outer envelope (not shown). Furthermore the outer envelope had nearly constant entropy, although the planet grew in mass and lowered its entropy, indicating the importance of the recycling-mediated accretion, as in Ormel et al. (2015) and subsequent works (Cimerman et al. 2017; Kurokawa & Tanigawa 2018).

By the time of 10 orbits, or 120 years, the low-opacity Neptune had accreted 1 $\mathrm{m}_\oplus$ of gas, and the high-mass has 0.3 $\mathrm{m}_\oplus$ of gas in its envelope. Relative to the core-mass, those are the highest values for all the simulated planets and already encouraging results for future simulations aiming to accumulate significant gas fractions without the snapshot approach. Those simulations should be improved by running them with deeper r_s, the Semenov et al. (2003) & Malygin et al. (2014) opacities and stellar heating, in order to check the influence of those parameters on the planetary growth. A variable adiabatic index γ, however does not seem to be necessary, for the low planetary masses to trigger high accretion rates (Piso & Youdin 2014; Piso et al. 2015). Those works explain that contrary to expectations, the lowering of γ through hydrogen dissociation, does not lead to an early unstable envelope collapse like expected from star formation, due to inhibition effects through the solid core.

3.4 Intermediate masses: Optically thin gaps and baroclinic envelopes

The next important pit stop along the growing masses of protoplanets are the Saturn-masses (95 $\mathrm{m}_\oplus$) which were studied extensively in Paper I. In the context of the previous discussions, those planetary masses are important because they open partial gaps in their parent discs and contract their envelopes significantly, compared to the 20 $\mathrm{m}_\oplus$-planets. This leads to the formation of optically thin gaps, or equivalently said, an enclosed photospheric surface around the $\kappa = 0.01\,\mathrm{cm}^2\,\mathrm{g}^{-1}$ Saturn-mass planet.

The fact that this surface is enclosed, and hence the planetary envelope can be regarded as a strange, deformed star, was helpful in measuring the luminosity L_1 through the summation of blackbody contributions on the post-factually computed $\tau = 1$-surface. Furthermore, the actual cooling fluxes from FARGOCA were extracted which, after solving some geometric intersection problems, which

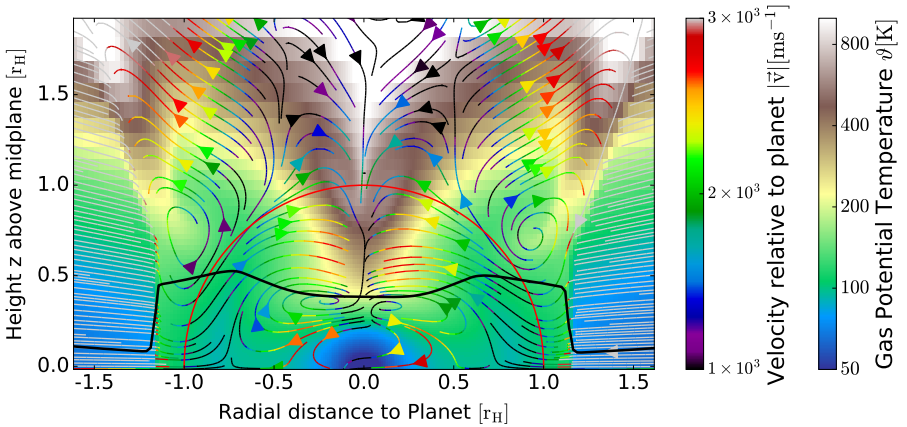

Figure 3.6: Vertical 2-D cut through flow vectors, with absolute velocity as colours in the envelope of a Saturn-mass planet. The black line denotes the $\tau = 1$-surface for this $\kappa = 0.01\,\mathrm{cm^2\,g^{-1}}$ run. The gas potential temperature or entropy is painted as background colour. Vortical flow structures are becoming evident at entropy saddle points, given by the baroclinicity of the envelope. Note that the flow has important components perpendicular to this plot, and hence a seemingly closed vortex loop, will effect in 3-D in a swing-by with torsion. This shows that density-temperature structures will cause flow structures and not the other way around.

gave another luminosity value L_2. Beyond that, the accretion rates through the increase in mass were measured, which can be translated via Equation 3.3 into the luminosity required by this given mass accretion L_{acc}. All three values were within 20% agreement, which underlines that the understanding developed earlier in this chapter is correct. Furthermore it established trust into the envelope solutions which were not as simple to analyse.

A question which those planetary masses permitted to investigate is the following: What role does the shape of flows play for the gas accretion rates? Are they cause or effect of accretion?

This question arose, as it is a popular method to derive accretion rates from isothermal simulations with a sink-cell at the planetary position (Kley et al. 2001; Machida et al. 2010; Tanigawa et al. 2012; Tanigawa & Tanaka 2016; Sanchis et al. 2020). This sink cell extracts a fraction or the entirety of its gas density contents per timestep and hence creates a vacuum, that the planetary envelope solution will

attempt to fill in the next timestep. Therefore, based on how much gas refills this sink cell, an accretion rate into the planet is measured. However, knowing the enormous density that isothermal solutions are able to build up from the preceding discussion, one may be sceptical about those accretion rate measurements. In this isothermal literature, one often finds a substantial focus of the discussion on the structure of the gas flows, because it is those flow structures that determine whether a planet can accrete or not, and what implications for the long-term angular momentum evolutions would be. Those accretion rates are *flow-dominated*, and it is found that the simulations in this thesis do not behave identically. The entire accretion process in this work is found to be determined by the compressional heat (and viscosity in the underresolved cases) of the envelope and its ability to radiate this heat away, as already laid out in earlier arguments. The gas cannot flow where pressure gradients are still too high, and hence the cause-and-effect situation reverses compared to isothermal simulations.

Furthermore, addressing the structure of flows, one could expect significant changes thereof in radiative envelopes, particularly once the disc surrounding the planet becomes transparent due to gap formation. The density-temperature structure in the planetary envelope necessarily must become baroclinic, as seen in Fig. 3.6, which poses a source for the flow vorticity $\vec{\omega} \equiv \vec{\nabla} \times \vec{u}$, where $\vec{u}$ is the gas flow vector, and it is,

$$\partial_t \omega \propto \frac{1}{\rho^2} \vec{\nabla} \rho \times \vec{\nabla} T. \tag{3.7}$$

As this type of flow can be subject to significant shear and compressional effects, it was interesting to quantify whether those factors can influence the envelope energetics, and hence accretion rates. Those effects were found to be negligible, again due to the same reasoning as before, namely the dominating effect of compressional work in a deep potential.

The message of this section might of course change in future work that would incorporate the effects of dust transport and their effects on radiation transport in those protoplanetary envelopes. The envelope cooling behaviour could become coupled to the gas flows via the relative efficiency of depositing high-opacity dust at specific radii around the planet. A very simplified approach to address this question was taken in this thesis, by simulating a limited set of Saturn-mass envelopes with Bell & Lin (1994) opacities. An interesting result from this investigation was a buoyant barrier-type convective region, just in the vertical at, the iceline location for a very dusty envelope. This is indicative that dust feedback processes might change the conclusions presented here significantly and require future work.

3.5 Jupiters and beyond

After a planet reaches the mass of Jupiter, its growth is classically expected to be truncated by the formation of deep gaps. While this idea, stemming from classical 1-D models has been shown not to hold up in 2-D simulations of equal planet masses due to gap-crossing flows (D'Angelo et al. 2003), it is still expected to be true at high enough planet masses, as the strength of gravitational torque densities that such a massive giant planet is able to exert on the surrounding gas, increases. In the simulations presented here however, no mass cut-off in the supply for Jupiter-mass planets is seen, only a change in the slope of the function $\dot{M}(M)$. This might be interpreted as the onset of the planets accreting at disc-limited accretion rates, as suggested by Bodenheimer et al. (2013).

Nonetheless it is instructive to compute the total growth timescales of the protoplanets presented in this thesis over the entire mass sequence from 20 $\mathrm{m}_\oplus$ to 360 $\mathrm{m}_\oplus$. This yields growth times via gas accretion of $\sim$150 kyr for $\kappa = 1.0\,\mathrm{cm}^2\,\mathrm{g}^{-1}$ and $\sim$20 kyr for $\kappa = 0.01\,\mathrm{cm}^2\,\mathrm{g}^{-1}$ from the gas accretion rates presented in Paper II. This seems like a reasonable short timescale, and expected from runaway gas-accretion models.

However there are free parameters in the simulations which were used in this work, and r_s is arguably the most important one. As any theory should strive to remove free parameters from its body, an investigation was started in Paper I in order to check how the too large size of r_s influences the gas accretion rates. When lowering r_s, the planetary potential is deepened and the gravitational compression becomes accordingly larger. This causes the internal energy content and the envelope luminosity to increase, but not in equal proportions. For a doubling of the potential depth an increase of only 1.5 in the luminosity is found. Following Equation 3.3, this predicts a lowering of the accretion rates, which is in fact measured. When this trend is extrapolated to more realistic planetary radii for hot protoplanets of 1-3 r_Jup (Mordasini et al. 2017), it is possible to find that the accretion rates would be decreased by a factor of 10-20, when employing the constant opacities. The Bell & Lin (1994)-opacities seem to possess an even steeper dependency with r_s. As the total duration of the gas accretion process will be controlled mostly by the low-mass accretion rates, this emphasizes that a future investigation should focus on a low-mass planets with deep, well-resolved potential, to settle this issue once and for all.

It is furthermore important to keep in mind that the growth timescales presented in this thesis have probably been further underestimated due to the value of the viscosity employed. As viscosity is responsible for delivering mass into the

planetary gap, which can subsequently be accreted, one expects a lower mass accretion rate for the lower viscosity which observations now impose.

From a number of unpublished simulations, it becomes clear that reducing either the viscosity or the disc mass by a factor of 10, lowers the gas accretion rates only by a factor of 3. Assuming a constant disc mass, 10 times lower viscosity, and applying the $\times 10$ correction factor for finite $r_{\rm s}$ would update the growth times to 30 times the previous values, hence the final estimates for the growth times of gas giants under those assumptions would be $\sim$4.5 Myr for $\kappa = 1.0\,{\rm cm}^2\,{\rm g}^{-1}$ and $\sim$0.6 Myr for $\kappa = 0.01\,{\rm cm}^2\,{\rm g}^{-1}$.

Adding 1.5 Myr waiting time for the core to assemble via pebble accretion (Morbidelli et al. 2015) and mass decrease during disc disperal, and contrasting this with the lifetime of circumplanetary dics, which is on the order of 3-5 Myrs (Haisch et al. 2001; Mamajek 2009), would naturally move high-opacity gas giant formation into a 'problematic' category and low-opacity gas giant formation into the 'possible' category, just as concluded in the literature (Hubickyj et al. 2005; Movshovitz et al. 2010; Mordasini 2014). Whether those numbers, scaling relations and correction factors can explain the low occurrence rates of cold Jupiters of 10% (Mayor et al. 2011), and whether there remains a need for fine-tuned planetesimal bombardment scenarios to delay gas accretion (Alibert et al. 2018) would have to be tested in a population synthesis code.

It seems interesting that the derived growth timescales can be just on the order of the disc lifetime. This would indicate that the two processes are in direct competition, and a piece of missing physics might be responsible for tipping the balance in favour of low gas accretion rates and hence low occurrence rates. In the light of this, the reader shall be reminded about the arguments laid out in Manara et al. (2018) indicating that circumplanetary disc masses do not seem to be sufficient enough to form the observed exoplanetary system masses. One of the solutions those workers proposed was that accretion discs are even more dynamic than was previously thought, quickly deorbit into the star and are replenished with fresh material from the surrounding cluster environment. Therefore, at the end of this part about accretion, it shall be speculatively proposed that the either episodic or coherent accretion of fresh intracluster medium would deliver ISM-like, high-opacity dust into the circumplanetary disc, pollute it, and hence delay gas accretion, to tip said balance of timescales.

This concludes the presentation of the thesis work on gas accretion rates, and it shall now be moved on to two follow-up projects that concerned this thesis work, which were addressing studies of circumplanetary discs around gas giants.

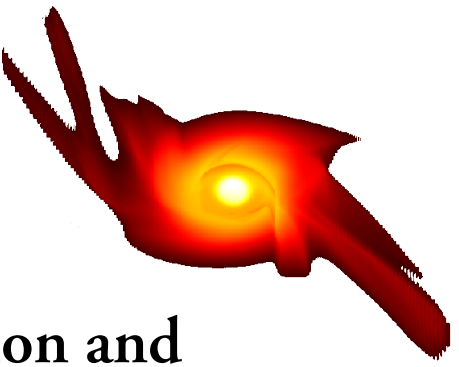

Chapter 4

Structure formation and observability at Jovian masses

As nature is inherently three dimensional, a spherically symmetric collapse or accretion of gas onto protogiants is very unlikely. Simple physical considerations of the conservation of angular momentum as well as simulations (Kley et al. 2001; D'Angelo et al. 2003; Ayliffe & Bate 2009a, 2012; Tanigawa et al. 2012; Szulágyi et al. 2016) show that the gas accreted by the Hill-sphere of a giant protoplanet must first shed its angular momentum with respect to the planet somehow, or it will inevitably form a circumplanetary disc, in the same way as circumstellar discs are formed around their host stars. Furthermore, once those circumplanetary discs reach a significant fraction of their orbital *and* local sound speeds, they will form separate sets of spiral arms via the nonlinearized perturbations by the stellar tidal field (Zhu et al. 2016), which is still felt inside the planetary Hill-sphere. Those processes are in the widest sense what might be called the formation of structures in protoplanetary envelopes. A tentative investigation of the envelopes of the Jovian mass planets in the data set presented in this thesis seemed to indicate the formation of structures, which were then followed up.

Furthermore, recent observations point to a low numbers of suspected (Sallum et al. 2015; Quanz et al. 2015) and confirmed protogiants (Keppler et al. 2018; Haffert et al. 2019) with possible circumplanetary discs surrounding them (Isella et al. 2019), hence yielding the possibility to observe structures. The observability of structures in outer protogiant envelopes became the focus for the last part of the thesis work presented here.

In order to correctly simulate the physics of the circumplanetary disc, a high

numerical resolution is required not only inside the smoothing length, as was discussed previously, but as well in the entire Hill-sphere. While classical 'factor-2'-mesh refinement provides very accurate means to resolve spherically symmetric envelope structures down to planetary cores, FARGOCA features a different grid geometry, that of a nonuniform gridding in which every cell has always six neighbours. Additionally there is no strict requirement on how rapidly to increase the resolution when approaching the planet, so there was room for experimentation and the possibility to resolve the entire Hill-sphere quasi-uniformly, while keeping the computational cost reasonable.

The results of those thoughts and experimentation led to the articles Paper II and Paper III.

4.1 Circumplanetary discs and their properties

There are several clues that speak for the existence of circumplanetary discs during the planet forming process, and their role in moon formation.

The low specific angular momenta of solar system giant planets (Bodenheimer 1977; Cameron 1988) and exoplanets (Bryan et al. 2018) do suggest an angular momentum sink must have existed between the circumstellar disc gas and the giant planets whose rotation rates we can probe. This mechanism has been proposed to be due to the mediating action of a circumplanetary disc (Takata & Stevenson 1996; Batygin 2018).

Furthermore, the co-orbital properties of the solar system satellites orbiting the giant planets are often taken as evidence for their common origin in a rotating circumplanetary disc (Coradini et al. 1981; Canup & Ward 2006) similar to those circumstellar discs discovered in the recent decades.

Lastly, the increasing iciness of the Galilean moons with their distance from Jupiter (Stevenson 1985; McKinnon 1987) is often interpreted as clue that the moons formed in the orbital sequence we can observe them today, which would have given rise to a larger accretion of ices at large outer radii in a putative gaseous disc.

Of the results presented here, the spontaneous formation of a circumplanetary disc in a low-opacity envelope is one of the most interesting ones, as shown in Figure 4.1 and this provides the opportunity to study this object. Despite central planetary temperatures exceeding 1.3×10^4 K, the planetary envelope collapsed, contrasting with an earlier claim by Szulágyi et al. (2016), that it is the central temperature which controls the formation of circumplanetary discs.

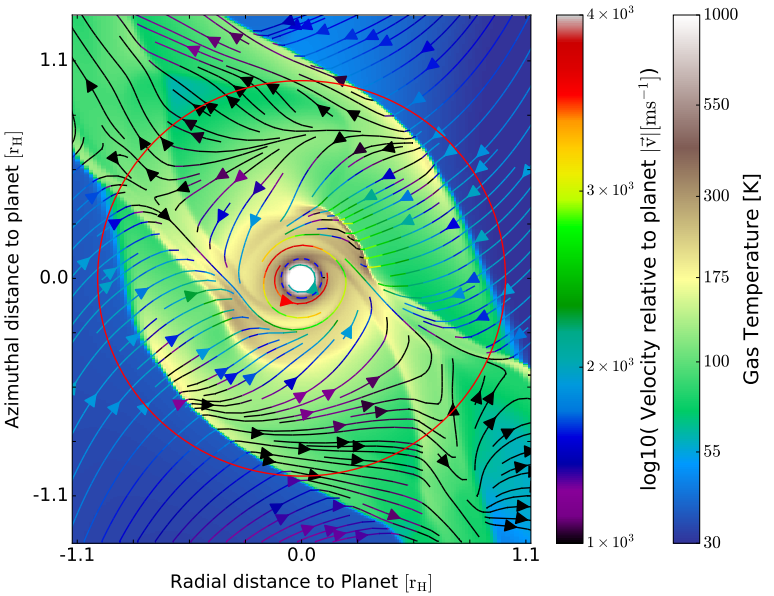

Figure 4.1: Gas streamlines and temperature as background colour in the envelope of a Jupiter-mass planet which successfully formed a circumplanetary disc. The temperature emphasize features, such as the spiral arms in the circumplanetary disc.

An overall view of the flow structures found in the simulations for the Jovian-mass of both high nand low-opacity envelopes can be seen in Fig. 4.2. The high opacities accrete a majority of their gas from the top layers of the circumstellar disc and generally from radii r-$r_{\rm P}$ close to the planet, i.e. angular momentum poor gas. Furthermore the high-opacity case does not form a circumplanetary disc.

The circumplanetary disc and its environment form a complex ensemble which is discussed in-depth in Paper II, but the most important findings shall be summarized here. The circumstellar gas can push past the spiral arm, eroding it, but being partially replenished with mass via vertical mass delivery. After gas passes the circumstellar spiral arm, it free-falls onto the circumplanetary disc and triggers a midplane accretion shock. The circumplanetary disc develops its own set of spiral arms, which act to kick the gas to high fractions of the orbital speed $v_\theta/v_{\rm Kepler} > 0.9$, unlike the spiral arms presented and discussed in the circumplanetary discs in Zhu et al. (2016), which resultsed in active accretion of the disc onto the planet. Because of those spiral arms, the gas orbits, but rises above the

circumplanetary disc midplane after a few tens of orbits in the disc, and is then accreted into the planet. This shows how the total accretion flow of a protoplanet can be processed through the circumplanetary disc at low opacities, and contrasting this, will fall onto the planet without passing through the midplane, at high opacities. The question remains open whether other self-consistent radiative simulation setups exist which would exhibit mixed features, i.e. with circumplanetary discs but mostly vertically accreting, such as seen in isothermal simulations.

In general, only a very small fraction of the gas entering the circumplanetary disc remains in orbit around the planet and contributes to its mass growth. Still, given the measured low accretion rates in Paper II ($\sim 10^{-7}\, m_{\oplus}\, yr^{-1}$ in dust, when assuming a dust-to-gass ratio of $1/100$), the disc can reach sufficient mass in solids to form the Jovian moons in 0.1-0.3 Myr, assuming a constant dust-to-gas ratio throughout the solar system evolution.

The interpretation of those numbers and simualations is to be seen critical. Depending on the temperature, different particle sizes in a particle distribution can correspond to the chosen constant opacities. At temperatures of T$\approx$ 200 K, it would be sensible to use for $\kappa_{\mathrm{R}} = 1.0\,\mathrm{cm}^2/\mathrm{g}$ particles of about 10μm in size, and for $\kappa_{\mathrm{R}} = 0.01\,\mathrm{cm}^2/\mathrm{g}$ the dust would be about 1 mm in size. If it is assumed that only those particles make up the entire dust mass, then the mm-sized particles would drift towards the planet via the circumplanetary disc, and the 10μm particles would never get the chance to become moon forming material due to the lack of a circumplanetary disc.

Hence, those simulations clearly do not provide the final answer yet as to how moon-forming material can enter and remain in the circumplanetary disc. Furthermore, the conditions in the early solar system might not even permit for dust, large or small, to pass beyond the planetary gap in the circumstellar disc (Ronnet et al. 2018) and require delivery by grown planetesimals (Canup & Ward 2006; Ronnet & Johansen 2020). Last, but not least, differences in flow structures can have chemical and observable consequences. Because the disc chemistry allows for a veriety of ices to exist at different vertical positions above the disc midplane, the composition of a giant planet will change depending on whether most of its gas is accreted from the midplane or the upper disc. In a recent work, Cridland et al. (2020) showed different outcomes in the overall chemical makeup of a giant planet to be dependent on the vertical accretion mode. Future simulations of envelope structures will require size-resolved global dust transport models in order to clarify the duration of the individual phases of top- or midplane-accretion, when taking dust coagulation and settling self-consistently into account.

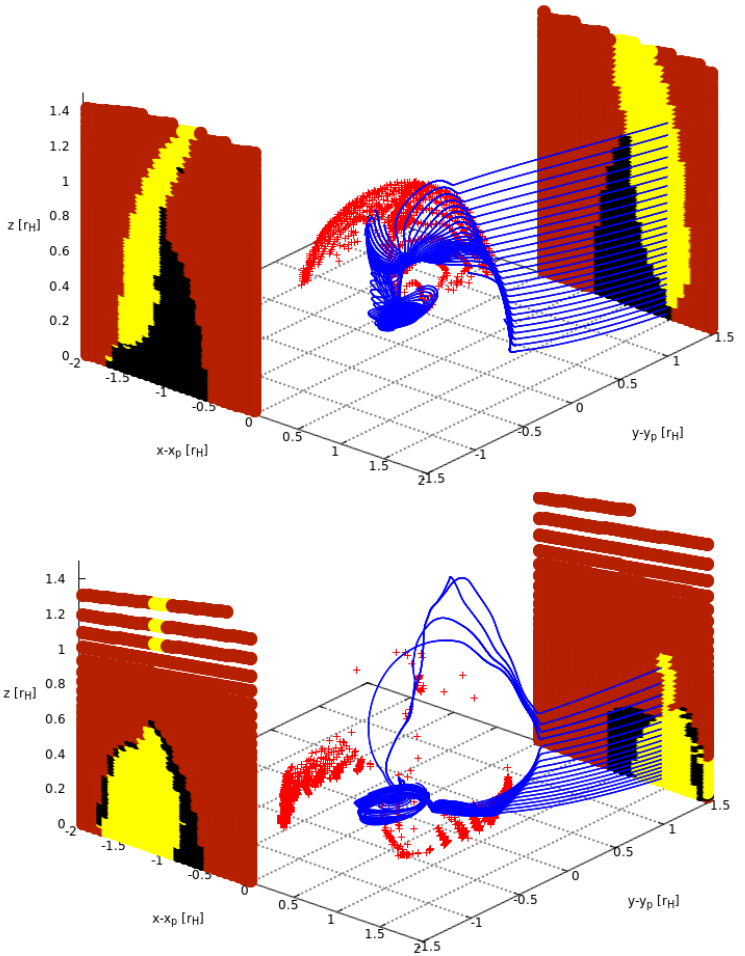

Figure 4.2: Large-scale accretion structures, high opacity ($\kappa_{\mathrm{R}} = 1.0\,\mathrm{cm}^2/\mathrm{g}$, *Top*) versus low opacity ($\kappa_{\mathrm{R}} = 0.01\,\mathrm{cm}^2/\mathrm{g}$, *Bottom*) for the Jupiter-mass planets. Streamlines following the gas motion are depicted in blue. The streamlines start at opposing sides of the Horseshoe region and are only examples of the entire sampled volume. Only the starting-points of streamlines as function of their accretion outcome are coloured: Yellow starting points are accreted streamlines, black points are passing streamlines, i.e. entering and exiting the Hill-sphere and bordeaux points are particles that are neither. Red cloud points show where accreted streamlines pass closer than $0.75\,r_{\mathrm{H}}$. It becomes evident how for the low opacity most of the gas is accreted from close to the midplane and passes through the circumplanetary disc, and for the high opacity accretion comes from the top into the Hill-sphere and the upper disc layer.

4.2 Dust in the envelope: Observational properties & an attempt at self-consistency

The last project in this thesis was concerned with the study of observational consequences of dust growth in protoplanetary envelopes. A recent claim of a putative circumplanetary disc around PDS 70 c (Isella et al. 2019) piqued this author's interest and served as motivation to model the infrared to submm spectra emitted by the circumplanetary simulation data presented in the last paper. While Isella et al. (2019) used an opacity value in the submm more akin to μm sized dust, they reported a dust mass in mm-sized particles. This was found to be too confusing by this author, hence an initial investigation was launched, which escalated into a full paper. The key idea to approach this project was to keep the undertaken assmuptions about mean opacities in the hydrodynamical simulations as consistent as possible with the dust populations employed. Details of the methodology and the results can be found in Paper III, but the process shall be summarized here.

As rough guides, the high opacity value $\kappa_{\mathrm{R}} = 1.0\,\mathrm{cm}^2/\mathrm{g}$ was computed to be a match for particles of about 10μm in size, and the match for $\kappa_{\mathrm{R}} = 0.01\,\mathrm{cm}^2/\mathrm{g}$ was computed to be particles of about 1 mm in size. The effect that dust growth decreases its opacity is well-known (Ossenkopf & Henning 1994; Henning & Stognienko 1996; Beckwith et al. 2000) and has been explained before.

However, as the real opacities of the components that constitute interstellar dust are not just constant values. They represent real minerals, carbonates and ices with varying responses to electromagnetic radiation, and can grow into a variety of 3-D geometries (Güttler et al. 2019). For the sake of simplicity, spherical dust was assumed throughout Paper III. The laboratory data needed in order to obtain dust opacities was the complex refractive index, taken from the Heidelberg-Jena-St. Petersburg database of optical constants (Henning et al. 1999). Those optical constants were be translated into opacities by solving the Mie-scattering problem, i.e. one treats the material with the optical constants in question as substrate and then irradiates it with electromagntic plane waves at wavelengths of interest. Results can be obtained using numerical (e.g. Bohren & Huffman 1983) or analytical solutions (Pollack et al. 1994).

Once the opacities are known, one uses them alongside with the density and temperature data from the hydrodynamic simulations as input for the full radiative transport solver *radmc3d* (Dullemond et al. 2012). Now the reader might be confused, as the results in FARGOCA are already obtained by solving the radiative diffusion problem. The difference is, that the full radiative transport problem

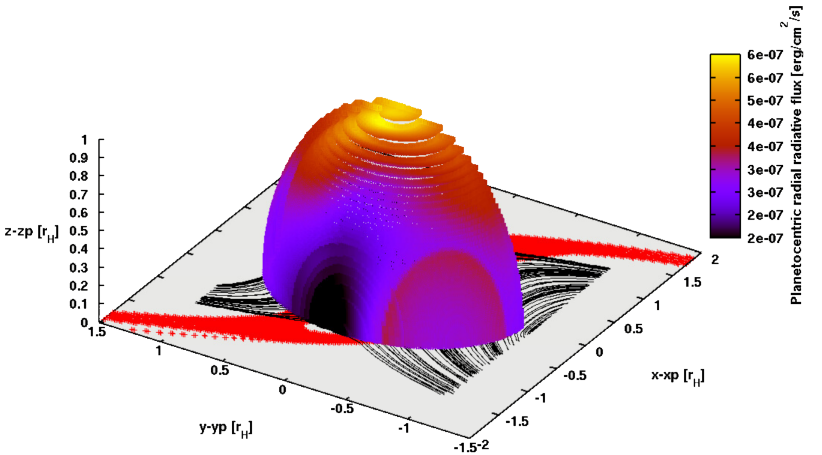

Figure 4.3: Example 3-D rendering of the planetocentric radiation flux vector $\vec{F}_{\rm P}$, projected on a half-sphere with radius $r_{\rm H}$ a Jovian planet at low opacity. Overplotted are the midplane of the circumstellar disc, denoted as x and y, with a few helpful orientation markings: The Horseshoe-orbits in black, and the background midplane density in a range of $10^{-12} < \rho\,[g/cm^3] < 3 \times 10^{-12}$ denoted as red points in order to show the position of the circumstellar spiral arms in the midplane. It becomes clear how gas that follows the horseshoe orbits heats the protoplanetary envelope as it crashes into the spiral arms, evident as bright half-ring. Furthermore the spiral arms, through their increase in density and hence optical depth, provide obstacles for the cooling fluxes, evident as dark areas. The top layers of the envelope present a hot spot as photons escape into the disc atmosphere. High opacity simulations possess similar overall features as presented here, but a much larger ratio between the midplane and vertical fluxes of about $\sim$30.

computes the transport of 'brightness-rays' or individual photon packages. As this is often difficult to compute due to the, in principle, infinite angular resolution required in order to compute the transported total amount of energy, moment-based methods are very popular in their usage (Mihalas & Mihalas 1984). The zeroth moment of the brightness is the photon energy density, and the first moment is the photon energy flux. The latter are less precise, but orders of magnitude faster in their computation, and the flux-limited diffusion (Levermore & Pomraning 1981) that FARGOCA employs is a zeroth moment-based method in the implementation of Commercon et al. (2011).

Therefore, while one method is exact, but the other one is fast, it is not practical to make them work together for time-dependent, high-resolution, fully self-consistent radiative solutions. This also means that my only option was to process data snapshot which were found in an approximate steady-state. Despite those caveats and limitations, it is still instructive to inspect the state of the radiative variables in FARGOCA, formulate rough expectations, and compare those to synthetic images generated by radmc3d.

The radial components of the radiative fluxes for an example planet are presented in Figure 4.3, where they are projected onto the surface of its Hill-sphere. The top of the Hill-sphere shows a clear hot-spot where cooling is most efficient due to the low optical depth. Closer to the midplane the fluxes decrease due to the higher optical depth of the envelope, spiral arms and the material on Horseshoe-orbits.

A resulting synthetic image, for which a far superior spatial imaging resolution to ALMA is assumed, can be seen in Figure 4.4, which is taken near the maximum wavelength of emission of the vertical hotspot[1] and is located at 8 μm. This image corresponds roughly to the expectations from Fig. 4.3, but this is only because the emission surface at this wavelength was chosen such it that possesses a particular shape and intensity contrast.

Note that particularly the contrast decides whether features would be actually observable at a given wavelength, even with the assumed high spatial imaging resolution, and contrast dictates the necessary observation time. Hence, a significant number of years will have to pass in order to see any such structure in real observations. Barring spatially resolved structures, one has to resort to traditional astronomical methods and learn from spectra, which can be thought of as summed-up wavelength-dependent images and are presented and explained in Paper III.

As initially stated, the aim of this project was to match hydrodynamic data with corresponding average dust opacities. This condition can be relaxed, when matching average optical depths instead, as it allows one to explore how spectra at constant optical depth would change when dust grows via a prescribed change of density. At the same time this opens up the possibility of increasing the dust-mass in the circumplanetary disc, in a way that the speed of the hydrodynamic simulations would not allow.

This led to an investigation into the behaviour of spectral shapes in the far-

[1]Note that the maximum position in the distribution $\lambda F_\lambda = \nu F_\nu$ will give the same value, independent of wavelength or frequency, $\lambda_{\max} = 3.5\,\mathrm{mm\,K/T}$.

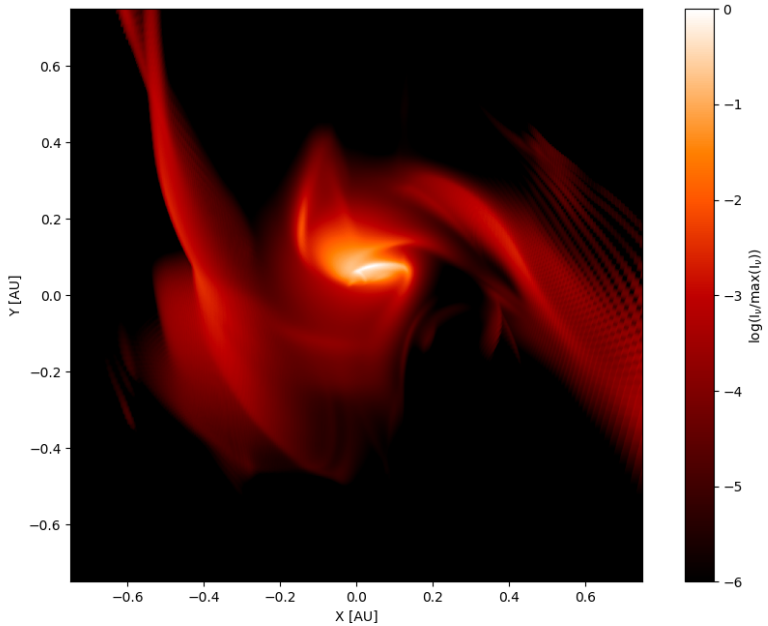

Figure 4.4: Synthetic observations of the low-opacity Jupiter-mass planet seen at 50° inclination, to serve as PDS 70c mock-up. This image has been post-processed at a wavelength of 8 μm using only 1 μm-sized Olivine dust as opacity source. The rough outline of features from Fig. 4.3 is reflected in this image. The planet is located at $(0, 0)$. Note how the position of the hotspot is offset from the planetary position. This is because the optical depth of the surrounding envelope extends the emission surface to temperatures at which the envelope is too cold to radiate efficiently. The hot spot which is located above the planet emits at $\sim$400 K, which possesses its energy emission maximum at $\lambda F_\lambda \sim 8.8\,\mu$m.

infrared and sub-mm spectral slopes as the dust grows. Briefly, large dust of mm-sizes will not present itself with any spectral features, it is *grey*, contrary to what one would expect from sub-μm sized dust in the interstellar medium. Furthermore mm-sized dust produces very broad spectra, which are able to fit the spectrum of PDS 70c, while keeping the contraint that the sub-mm emission is dominated from the CPD. The latter is necessary because the models overestimate the planetary contribution to the spectrum, hence, a spectrum that is planet-dominated and would fit the data, would not fit it anymore after the hydrodynamic models are improved.

Therefore, mm-sized dust, after increasing the dust mass 30-fold, seems to be on one hand, consistent with the formation of circumplanetary discs and on the other hand with the spectral data of the object PDS 70c. While not entirely unexpected, as already class I objects show indirect signs of grown, mm-sized dust (Harsono et al. 2018), it is nonetheless an important piece of information for further purposes of providing the building blocks of moons in theoretical models.

The presence of smaller particles in PDS 70c is a possiblity, but this would require higher dust masses to fit the data, as was explored in the last part of Paper III. The spectrum seems to be able to be fit as well with vastly increased dust masses of 1 μm and 10 μm particles. The only preference which exists on the dust masses is the analysis in Isella et al. (2019), hence it is prudent to be agnostic and not exclude even high dust masses.

In the parameter space of circumplanetary disc masses, viscosities and complex opacity models, there is certainly still unexplored volume, hence no claim shall be made for those fits to be unique, but they are certainly a first step in using more realistic 3-D settings to model observations.

Chapter 5

Numerics

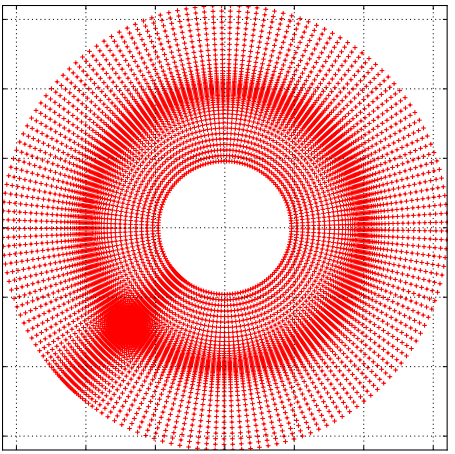

A large part of non-physics based work during the execution of this thesis related to numerical and code execution speed issues. The code was mostly working well and so remaining work focussed on decreasing the long waiting times in the code exploitation. Significant effort went into finding optimal hardware and grid configurations in order to run the code, as is presented in this chapter. An example of a Gaussian grid structure, introduced later in this chapter, is shown on the top right of this page.

Depending on the problem setup, global 3-D radiation hydrodynamics simulations can nowadays run hundreds of orbits in a reasonable runtime of days until weeks. However the aim of this thesis was to investigate as deep as possible into the protoplanetary envelope, while keeping the simulation domain global. 'Deep' would mean here to use a as small value of the smoothing length as possible. This premise in itself guaranteed that some new limits on the computing time would be encountered sooner or later. Furthermore, of the key findings in Paper I, the fact that numerically convergent accretion rates and envelope structures require 10 grid cells per smoothing length, contributed significantly to encountering those limits. Now for purposes of documentation, first the used hardware shall be presented, before continuing to discuss numerical techniques in the simulation code.

Essentially all simulations were run on the LUNARC-hosted machine Aurora. Aurora is a distributed computing network (commonly referred to as a 'cluster') of 230 computing nodes. Each computing node consists of two Intel Xeon E5-2650 v3 processors, with 2.3 GHz clock rate each and 10 computing cores for each processor. Two 20 execution units each share a 64 GB bar of DDR4 RAM. We mention those hardware structures, as they have important consequences for

the behaviour in execution speed of FARGOCA.

FARGOCA is a parallel hybrid code. Hybrid codes use techniques of both shared memory (OMP) and distributed memory (MPI) in order to divide up the work load of operating on several million hydrodynamic cells. The shared memory between the two processors on a node usually should prove non-critical for the purposes of execution time. However, once more nodes are in use, the MPI communication between nodes, for which data has to physically leave the processor chip, can incur penalties on the execution time. This is particularly critical for very heavy simulation setups, as the MPI buffer that listens to incoming data from the infiniband communication has a limited size, and if filled during non-blocking communication attempts, the corresponding CPU might idle for precious microseconds. While the common MPI-wisdom is that a good hybrid programm will usually spend 50% of its time computing and 50% of its time communicating, it is possible to check this ratio with Intel tools like the VTune Amplifier or the Intel Advisor, and take steps in case of bad performance.

Once a number of nodes to work on is chosen, there exists another free parameter to optimize speed, which is the number MPI-Tasks and OMP-Threads that should multiply to a total of 20 in order to fill a node. The optimal configuration for the number of Tasks$\times$Threads has to be found by scanning the entire configuration space, as the actual performance of any node+code combination can differ significantly from what could be expected when studying the node specification. A benchmark pipeline was created for this purpose, which automatically generates test simulations, input parameter script, SLURM scripts, couples and runs those, reads out execution times, corrects for start-up bias and can be repeated to reduce execution noise. An example of unexpected performance behaviour is shown in Fig. 5.1. Furthermore, the same figure shows an example benchmark process of how to find an optimal configuration at lowest cost to the CPU-hour budget of the entire human group sharing the limited available core-hours.

Minor speed-ups were further achieved by scanning through the benefits of static and dynamic scheduling in OMP loops, each with chunk sizes of 2-6. Dynamic scheduling on the main radiative loop with 2 chunks to schedule proved to be $15\% \pm 5\%$ faster than the automatic chunk size detection, and static scheduling about $7\% \pm 5\%$ faster. Hence, it might be worth exploring the effects of running all key OMP loops with dynamic scheduling in the new code, scheduled to be presented in mid-2020. Activated hyperthreading did not affect execution speed.

The simulation substeps used to generate initial as well as boundary data shall now be introduced. For full detail, see Paper I.

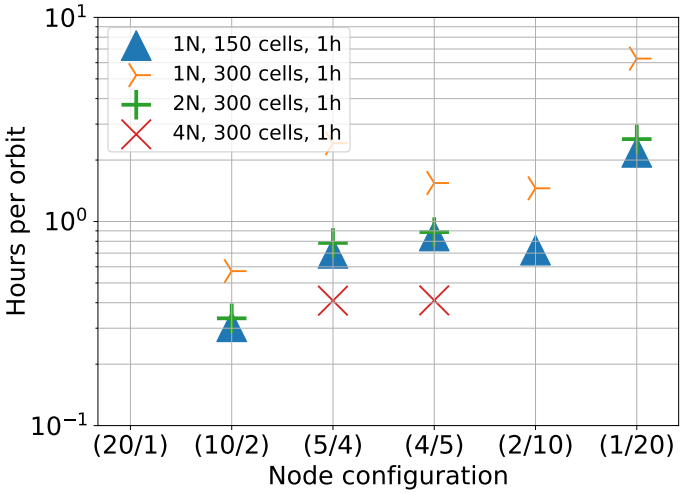

Figure 5.1: Typical scan through the (Nodes/Tasks/Threads) parameter space to find an optimal configuration during a step B run. The x-axis for both plots shows (Tasks/Threads) or (T/T). Times are measured for a setting with $N_r \times N_\theta \times N_\phi = 150 \times 768 \times 32$ cells and $N_r \times N_\theta \times N_\phi = 300 \times 768 \times 32$ cells respectively, with the radial direction being so far the only parallelized direction in FARGOCA. Hence the 150 or 300 radial cells are divided up amongst Nodes$\times$Tasks total tasks, and each task has to host at least 20 radial cells. Due to this, several configurations from (N/T/T)=(1/20/1),...(4/10/2) are unavailable. The top plot shows the startup time in seconds, the bottom plot shows the startup-time cleaned execution time for one orbit in hours, for a typical step B, gap forming run. From simple hardware considerations one would expect (T/T)=(2/10) to be the fastest configuration, but we find it to be (T/T)=(10/2), and use it whenever possible. The plot shows furthermore the following for the chosen setup: The penalty for doubling the radial cell-sizes can be offset by doubling the node number. When doubling the nodes to 4 nodes, the code scales well, but due to the 20 cells per task requirement, the fastest configuration becomes unavailable. Hence, this setup would be executed with (N/T/T)=(2/10/2).

5.1 Steps A,B,C - Generating initial and boundary data

The rationale for those substeps was already used in Kley et al. (2009), Bitsch et al. (2013), Lega et al. (2014).

The substeps are defined and sorted according to the timescales of physical processes in the circumplanetary disc. Step A finds the global, radiative equilibrium of a disc without planet, which can take a significant number of orbits to achieve. Depending on the exact nature of the heat sources and the opacity law used, nonuniform heating & cooling can trigger complex disc flows which transport mass, which feeds back into the energy transport properties. This feedback loop might take some time to find an equilibrium. Hence the disc equilibrium step is run in 2-D in radius and co-latitude to find this equilibrium quickly.

Subsequently, in Step B, the planet is introduced. This step forms the spiral arms and the gap, according to the physics explained in Chapter 2. Spiral arms are formed on a timescale of $\sim$orbits due to their nature originating in co-rotational resonances. Subsequently the long process of spiral-arm aided gap formation begins. The length of this process is defined by the viscous timescales, which at our chosen $\nu \sim 10^{-15}\,\mathrm{cm}^2\,\mathrm{s}^{-1}$ correspond to thousands of orbits, which necessarily have to be run in 3D. Significant gap depth can already be achieved after a few hundreds of orbits, shown to be already in a slowly convergent regime in Paper I, hence we usually truncate Step B after 400 orbits.

Step C is the high resolution run, which, as analyzed in-depth in the same article, provides the required numerical resolution in order to allow for gas accretion to occur. This process needs to run however only for about 5-10 orbits before the interesting results are measured. At the beginning of this thesis Elena Lega had finished implementing the nonuniform grids in FARGOCA. Those grid structures (one example is plotted at the entry of this chapter) allow high resolution inside the planetary Hill-sphere, but are different from classical factor-2 resolution, in that they can possess arbitrary resolution gradients. This allows for some important freedom in designing and optimizing the grids for execution speed.

It shall be noted that it is prudent to repeat the process depicted in Figure 5.1 for each significantly new workload configuration, as again the hardware can react in unexpected ways.

5.2 Short timescales and numerical methods to handle them

5.2.1 Advection-dominated problems: FARGO

FARGO (Masset 2000) stands for Fast Advection in Rotating Gaseous Objects, and uses a reduced system of equations to circumvent a severe limitation on the CFL-criterion that is posed on the solution of discretized hyperbolic equations, such as the equations of hydrodynamics, in rotating Keplerian discs.

The CFL criterion states that the timestep Δt of an attempted solution to an example 2-D system of discretized hyperbolic equations on a grid of spacing Δx, Δy must fulfil

$$\Delta t \leq \min\left(\frac{\min(\Delta x, \Delta y)}{\max(u_x, u_y)}\right) \tag{5.1}$$

with the example 2-D flow velocity components u_x and u_y. Any timestep violating this criterion will lead to solutions that grow in a way as to violate the discretized equations and grow exponentially. Its automatic fulfillment is not a problem, as the severity of this criterion can be computed from the simulation data at any time, and the timestep determined.

Obviously two factors are implicated in causing a slow-down of the simulation speed, namely high resolution and large velocities. The former is given by the static simulation grids in this thesis, the latter is dynamic and changes at simulation time. Additionally, one dimension of the simulation can cause significant slow-downs for the entire domain, while velocities are much smaller in the other dimension. This happens in systems subject to a large global shear flow, such as in circumplanetary discs, where in the inertial frame velocities are large, but there is no frame of reference in which one can transform the shear in velocities entirely away.

Therefore, in such systems, the flow velocity $u(r_{\min})$ or $u(r_{\max})$ at the inner and outer boundaries of the simulation domain will usually play the role of defining the most restrictive timestep. This problem becomes more severe on spherical grids which are equally spaced in azimuthal angle, such as the one that circumplanetary disc simulations use traditionally (Stone & Norman 1992). There, the physical Δx is the smallest at the inner simulation boundary, and $u_y(r_{\min}) = v_{\text{Kepler}}$ largest.

The insight behind the FARGO-type transport is now that on a static, equidistant grid with periodic boundary conditions, which circumplanetary discs in the azimuthal direction traditionally were taken as, transport in that same azimuthal direction is trivial, and can be performed by a manual shift of initial conditions. Then, the original equations of motion are reduced by substracting the large speed of the azimuthal transport, leaving a small remnant speed, which allows a much larger timestep.

The reader might have noticed that this entire procedure resembles solving the azimuthal transport problem in a non-inertial frame, i.e. co-rotating with the planet and then enjoying reduced $u(r_{\min})$. Why this method became disfavoured is due to the lower numerical diffusivity of FARGO-type algorithms over

co-rotating frames, as explained in Nelson et al. (2000). Furthermore, the treatment of the Coriolis force can cause spurious oscillations when not treated conservatively (Kley 1998). In order to avoid those problems and due to the speed-up in orbital advection achieved, FARGO-type algorithms have prevailed in the last two decades and led to versions focussed on 3D radiation hydrodynamics (Bitsch et al. 2014; Lega et al. 2014) and 3D magnetohydrodynamics (Benítez-Llambay & Masset 2016).

The FARGO algorithm is mainly used in step B. Initially it was used in step C, but as will be discussed shortly, its use was discontinued due to the enormous cell numbers it imposes in azimuth at high resolution.

5.2.2 Transporting photons at the speed of light, but finite computational cost: Implicit flux-limited Diffusion

FARGOCA uses the flux-limited duffusion (Levermore & Pomraning 1981) in order to relate the first moment of the radiation transport equation, the Fluxes F to the zeroth moment $e_{\rm rad}$ and hence act as a closure relation.

While this approach recovers the diffusive approximation in optically thick media, it also allows for the solution of radiation transport into optically thin media. The timescale for optically thin radiative transport would be however prohibitive to any solution of the system, as the optically thin radiative energy equation $\partial_t e_{\rm rad} + c\nabla e_{\rm rad} = 0$ features an advective timestep with the speed of light dictating the CFL criterion. Therefore, the method of choice used is an implicit solution of the radiative transport problem as presented in (Commercon et al. 2011). This part of the code execution takes up 50 % of the total computing time in good cases, while scaling up dramatically when large flux gradients enter the domain. Those can originate in deep, accreting potentials, adding solar radiation, or large opacity jumps.

5.3 Communication-dominated problems, Abandoning the FARGO algorithm

Very high resolution (> 50 cells per $r_{\rm H}$ for Saturn-mass planets) with FARGO took a large toll on the computing time, and slowed the execution substantially.

Specificly, this occured in Paper I, when it was attempted to improve the resolution from $N_c = 50$ to $N_c = 100$ during the step C runs. At this point a resolution of $N_r \times N_\theta \times N_\phi = 300 \times 8400 \times 70$ (176 MCells workload)

was used, and the radial and co-latitudinal grids were non-uniform, while the azimuthal grid was uniform. An attempt at doubling in resolution would have resulted in $N_r \times N_\theta \times N_\phi = 300 \times 16800 \times 70$ (353 Mcells workload), whereas the radial and vertical resolution increase was absorbed in higher global grid resolution gradients in order to keep those numbers constant, the azimuthal cells had to double due to the specification of the FARGO-algorithm.

At this point, instead of the usual scaling of a factor 1.5-2 slowdown upon workload doubling, the execution time dropped by more than a factor 4. This was worrying, as it would prohibit even higher resolutions and therefore the convergence tests, fundamental to Paper I, to conclude. A check with Intel VTune Amplifier showed that the total workload was slowing down the radiation routine at an MPI_ALLREDUCE that is executed every single one of the many iterations of every timestep. Additionally, the number of iterations that the radiation solver needed in order to converge, scaled stronger than linear with the workload. This was a clear sign, that for this workload, FARGOCA entered a communication-dominated regime, and therefore this was a problem which would not disappear when trying to simulate even higher resolutions or similar workloads.

Furthermore, the output-files were getting really heavy on the hard drive: Their weight was 1.3 GB/file (determined via the resolution), with seven radiation hydro variables makes 9 GB per output. Several outputs per orbit were needed as Aurora allowed a maximum runtime of seven days per job. Therefore, at 10 orbits per simulation and 10 outputs per orbit, one simulation would weigh $9 \times 100 = 910GB$. Would Paper I have been finished under those specifications (assuming the higher and lower resolution runs weigh equally) all those simulations would have consumed about 20 TB, a significant part the disk space for the entire department at that time. Clearly, both for the sake of execution speed and disk space, some innovation had to be devised.

A simple solution which would kill two birds with one stone was to reduce the number of data communicated via MPI processes dramatically, so that the cpu time would once again be computation-dominated, and the data written to the hard disk less. The only way to achieve this, was to reduce the number of azimuthal cells dramatically. This again, while keeping the resolution in r_s constant, meant the need to use a nonuniform grid in azimuth as well, which necessitated to stop using the FARGO-algorithm for the Step C runs. The decrease of azimuthal cells had therefore to be large enough to outspeed FARGO. There was no worry about the high diffusivity of the classical advection solver, as the accretion rate runs would take only 10 orbits in order to measure the accretion rates. At first, equal speed

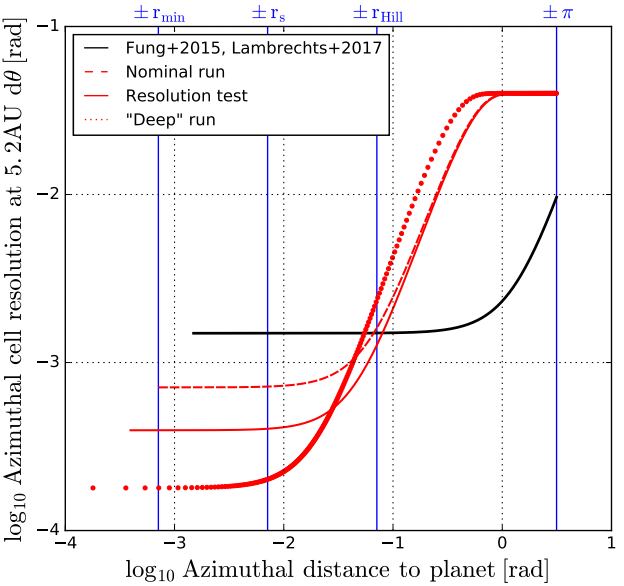

Figure 5.2: Example grid structures $d\theta(\theta)$ for the gaussian grid(s) and a previously used grid in Fung et al. (2015), Lambrechts & Lega (2017). A higher resolution grid and the grid for the deepest run, 'H2' in Paper II, are added

with the above quoted 176 Mcells workload was found at a new resolution of $N_r \times N_\theta \times N_\phi = 300 \times 1400 \times 70$ which is a workload of 29 Mcells and 240 MB per file. The azimuthal grid was the one used before in Fung et al. (2015) and Lambrechts & Lega (2017) with $d\theta \sim (\theta - \theta_P)^2$. With this, higher resolutions at only very moderate execution time decrease could be achieved and the convergence test could be finished at moderate disk usage, which led to several of the essential results in Paper I.

Later, following the doctrine to 'put the resolution where it is needed', the usage of grids of the form $d\theta \sim (\theta - \theta_P)^2$ was abandoned, and experiments with more extreme power indices and logarithmic grids were commenced. The former would lead to strange results, and the latter would lead to crashes of the code. The most viable solution seemed to be the usage of grids that would locally keep the old parabolic resolution profile around the planet, but would asymptotically approach uniform resolution outside of the Hill-sphere, in order to remain as consistent throughout the simulation domain outside the Hill-sphere as possible in the Step C run with the uniform resolution of Step B. Those were the Gaussian-type grids

introduced in Paper I. They are plotted for different resolutions of r_s in Figure 5.2.

The Gaussian grids were further optimized for the Jovian planet runs with an increase in resolution in co-latitude near the planet, which is required so that the vertical accretion shock would not crash the simulation upon restart. Additionally, an MPI bug was fixed, which prevented from simulating with more than 300 radial cells before. With this, the fast Task/Thread configuration discussed in Figure 5.1 became available again, increasing the speed further. The final configuration which was used for the high-mass runs in Paper II was $N_r \times N_\theta \times N_\phi = 350 \times 484 \times 124$, at a feather weight of 160 MB per file.

Thus concludes the report about the work on numerics in this thesis.

Conclusions

This thesis started out with a large question mark over how to accrete gas into the envelopes of protoplanets using the FARGOCA code. Prior works using this code that have studied those envelopes found their accretion rates to be zero within measurment uncertainties, although a mass increase should have been notable within simulation time.

After significant investigative work it was shown that gas accretion is possible, naturally occurs at high enough numerical resolution of the gravitational smoothing length, and shows numerical convergence. It was confirmed furthermore that the measured accretion rates are consistent with the expected gas accretion rates from Kelvin-Helmholtz contraction, usually thought to be the slow phase during giant planet accretion. The aspect of sufficient numerical resolution has furthermore significance for the density-temperature structure of protoplanetary envelopes, as it is found for those to show incorrect behaviour in underresolved cases.

After it was known how to accrete gas in a physically meaningful way, it was decided to perform a mass and opacity scan of the accretion rate parameter space. The accretion rates found proved to be consistent with earlier results in the literature, obtained with SPH codes, while our code was grid-based. Furthermore, a deeper investigation into the data revealed a significant change in the rotational properties of the accreted gas envelopes for high-mass planets. It was found that circumplanetary discs can spontaneously be formed in those envelopes only for low opacities, with a new and nontrivial mass delivery system providing the mass, which was investigated in-depth. Additionally, it was possible to characterize the flows and residence times of the gas in those circumplanetary discs, commenting on earlier hypotheses about circumplanetary-disc-modified gas accretion.

Finally, this work became focused on recent observations of accreting protogiants. The idea of distinguishing between high- and low-opacity accreting envelopes, translated into the idea of using dust populations which are consistent with those opacities. The subsequent modelling of spectral properties of the hydro-

dynamic simulations, showed that at least with the data given by the PDS70 observations, the models would favour mm-sized particles in the envelope of PDS70c for the nominally given dust mass, giving an important hint at dust-growth.

Future work must aim to restore consistency with observational results, particularly the ALMA data indicating low turbulent viscosity. Models with lower viscosity need to be run, which again require solar radiation to keep their hydrostatic structures from collapsing. As those steps are extremely expensive within the current numerical and hardware framework, new ways of improving simulation execution times must be devised in order to progress scientifically.

Chapter cover images and copyrights

Chapter 1: ©Juno mission, NASA/ESO, Public domain
Chapter 2: Protoplanetary disc with gap, own work
Chapter 3: Zoom on protoplanetary envelope in disc, own work
Chapter 4: Synthetic observation of a protoplanetary disc, own work
Chapter 5: Nonuniform grid structure used in this work, centered on the planet, own work

Author contributions

The next pages summarise the papers and my contribution to each paper included in this thesis.

Paper I:
Global 3D radiation-hydrodynamic simulations of gas accretion:
The opacity dependent growth of Saturn-mass planets

M. Schulik, A. Johansen, B. Bitsch, and E. Lega (2019)
Astronomy & Astrophysics, vol. 632, A118 (23 p.)

Summary:
This work firstly aimed to establish a functioning numerical framework of gas accretion onto protoplanets, before continuing to measure the opacity dependence of this process. For initially unknown reasons, gas accretion did not occur, although the gas giant envelopes were loosing energy through radiative cooling. We identified the crucial parameter to let gas accretion proceed to be the numerical resolution of the smoothing length. A numerical resolution study led to the finding of numerically converged accretion rates. The resolution study neecessitated the use of new grid structures in order to be viable in finite time. Furthermore the resolution study revealed two effects to be the deeper reason for this at low numerical resolution, the overestimation of viscous work and the inability of the radiative solver to cool. We then continued to explore the dependence of the gas accretion rates on constant opacities and found it to be surprisingly weak. Furthermore, using complex opacity models did not seem to affect the results substantially. In the face of abscence of analytical solutions for our set-up, we constructed a semi-analytical model to relate luminosity and gas accretion rate. This model helped to show that our results are physical and explained why the gas accretion rates decreased for increasing potential depth of the planet. The extrapolation of accretion rate against smoothing length gave us a correction factor that enabled us to estimate the true accretion rates of Saturn-mass planets.

Author contributions:
BB and AJ had the original idea to measure gas accretion rates with FARGOCA. BB and MS originated with the specific choice of planet mass. EL gave the decisive clue to identify the parameter inhibiting the gas accretion in conjunction

with a surprise finding by MS. AJ proposed the convergence test. MS initiated the use of Gaussian grids in order to save computation time for the convergence test. MS executed all simulations, analysed them and drew the conclusions. The paper manuscript was written by MS with significant help in structuring from AJ. img were produced by MS. The manuscript was improved and discussed with all coauthors.

Paper II:
On the structure and mass delivery towards circumplanetary discs

M. Schulik, A. Johansen, B. Bitsch, E. Lega and M. Lambrechts (2020)
Accepted in Astronomy & Astrophysics (19 p.)

Summary:
Considering the numerical limitations imposed on realistic simulations known from Paper I, we aimed to study the accretion rates to a wide range of protoplanetary masses. Preliminary studies of the envelope properties revealed an interesting transition in the rotational properties of the envelope between 120 and 240 Earth masses, indicating the formation of a circumplanetary disc. The study of the circumplanetary disc became the focus of the paper. On one hand we found spiral arm features and complex 3D flows inside the circumplanetary disc, proving that their occurence is not limited to 2-D setups. On the other hand we found gas in the midplane that free-falls onto the circumplanetary disc. This triggers a gentle accretion shock in the midplane, which has never been seen before. We confirmed the existence of this effect with numerical tests as well as with a more realistic set of opacities. The analysis and physical understanding of the cause of the free-falling gas proved to be more complex than expected, and occupied us for the rest of the paper.

Author contributions:
AJ, BB and MS had the original idea for the mass survey. MS ran the simulations. MS took the decision to focus on understanding the envelopes of the jupiter-mass

planets after visiting a conference on moon formation. MS identified the free-fall region as interesting nontrivial problem and performed the analysis. MS created the img and wrote the paper. The manuscript was improved and discussed with all coauthors.

Paper III:
The influence of dust growth on the observational properties of circumplanetary discs

M. Schulik, B. Bitsch, A. Johansen and M. Lambrechts (2020)
Submitted to Astronomy & Astrophysics (13 p.)

Summary:
In the light of recent protoplanet discoveries that are found in a (late) state of gas accretion, we decided to focus on the connection of theory and observation. Furthermore, we felt it necessary to comment on the seemingly inconsistent usage of mm-type particles for modelling of dust masses, but opacities corresponding to micron-sized grains in the literature. To this end, we post-processed our simulation data of circumplanetary discs from paper II with wavelength-resolved opacities and radmc3d. This was necessary as our simulations were only generated with average opacities, and would otherwise not have given us access to observable quantities. The wavelength-resolved opacities were taken to correspond to a standard mix of interstellar material, scaled up in size to correspond to our average opacities, in order to assure consistency with the average opacities of the hydrodynamic simulations. We find that when only mm-sized particles are present, this should leave a distinct imprint mainly in the far-infrared, while smaller particle sizes already bear an imprint of their 3D distribution. Finally, it seems that mm-sized particles are consistent with a 3 times lower mass in PDS 70c, than reported in Isella et al.(2019). Smaller dust sizes fit the spectrum for higher dust masses.

Author contributions:
MS and BB developed the original idea. All coauthors discussed with MS about dust properties. MS developed the software pipeline to use FARGOCA data with

radmc3d and our choice of dust species. MS created all the plots and wrote the paper. The manuscript was improved and discussed with all coauthors.

References

Alibert, Y., Venturini, J., Helled, R., et al. 2018, Nature Astronomy, 2, 873

Andrews, S. M., Huang, J., Pérez, L. M., et al. 2018, , 869, L41

Ansdell, M., Williams, J. P., van der Marel, N., et al. 2016, , 828, 46

Armitage, P. J. 2010, Astrophysics of Planet Formation

Aumann, H. H., Gillett, F. C., Beichman, C. A., et al. 1984, , 278, L23

Ayliffe, B. A. & Bate, M. R. 2009a, , 397, 657

Ayliffe, B. A. & Bate, M. R. 2009b, mnras, 393, 49

Ayliffe, B. A. & Bate, M. R. 2012, , 427, 2597

Ballering, N. P. & Eisner, J. A. 2019, , 157, 144

Batygin, K. 2018, , 155, 178

Beckwith, S. V. W., Henning, T., & Nakagawa, Y. 2000, in Protostars and Planets IV, ed. V. Mannings, A. P. Boss, & S. S. Russell, 533

Bell, K. R. & Lin, D. N. C. 1994, apj, 427, 987

Benítez-Llambay, P. & Masset, F. S. 2016, , 223, 11

Bergin, E. A., Hartmann, L. W., Raymond, J. C., & Ballesteros-Paredes, J. 2004, , 612, 921

Béthune, W. 2019, , 490, 3144

Bitsch, B., Crida, A., Morbidelli, A., Kley, W., & Dobbs-Dixon, I. 2013, aap, 549, A124

Bitsch, B., Izidoro, A., Johansen, A., et al. 2019, , 623, A88

Bitsch, B., Morbidelli, A., Lega, E., & Crida, A. 2014, , 564, A135

Bodenheimer, P. 1977, , 31, 356

Bodenheimer, P., D'Angelo, G., Lissauer, J. J., Fortney, J. J., & Saumon, D. 2013, apj, 770, 120

Bodenheimer, P. & Pollack, J. B. 1986, , 67, 391

Bohren, C. F. & Huffman, D. R. 1983, Absorption and scattering of light by small particles

Boss, A. P. 2000, , 536, L101

Bryan, M. L., Benneke, B., Knutson, H. A., Batygin, K., & Bowler, B. P. 2018, Nature Astronomy, 2, 138

Cameron, A. G. W. 1988, , 26, 441

Canup, R. M. & Ward, W. R. 2006, , 441, 834

Cimerman, N. P., Kuiper, R., & Ormel, C. W. 2017, , 471, 4662

Commercon, B., Teyssier, R., Audit, E., Hennebelle, P., & Chabrier, G. 2011, aap, 529, A35

Connelly, J. N., Bizzarro, M., Krot, A. N., et al. 2012, Science, 338, 651

Coradini, A., Magni, G., & Federico, C. 1981, , 98, 173

Crida, A., Morbidelli, A., & Masset, F. 2006, Icarus, 181, 587

Cridland, A. J., Bosman, A. D., & van Dishoeck, E. F. 2020, , 635, A68

D'Angelo, G., Kley, W., & Henning, T. 2003, , 586, 540

D'Angelo, G. & Podolak, M. 2015, , 806, 203

Debras, F. & Chabrier, G. 2019, , 872, 100

Dullemond, C. P., Birnstiel, T., Huang, J., et al. 2018, , 869, L46

Dullemond, C. P., Juhasz, A., Pohl, A., et al. 2012, RADMC-3D: A multi-purpose radiative transfer tool

Dürmann, C. & Kley, W. 2017, aap, 598, A80

Eisner, J. A., Arce, H. G., Ballering, N. P., et al. 2018, , 860, 77

Frank, J., King, A. R., & Raine, D. J. 1985, Accretion power in astrophysics

Fung, J., Artymowicz, P., & Wu, Y. 2015, APJ, 811, 101

Goldreich, P. & Tremaine, S. 1978, , 222, 850

Goldreich, P. & Tremaine, S. 1980, , 241, 425

Grether, D. & Lineweaver, C. H. 2006, , 640, 1051

Güttler, C., Mannel, T., Rotundi, A., et al. 2019, , 630, A24

Haffert, S. Y., Bohn, A. J., de Boer, J., et al. 2019, Nature Astronomy, 3, 749

Haisch, Karl E., J., Lada, E. A., & Lada, C. J. 2001, , 553, L153

Hanel, R., Conrath, B., Flasar, F. M., et al. 1986, Science, 233, 70

Harsono, D., Bjerkeli, P., van der Wiel, M. H. D., et al. 2018, Nature Astronomy, 2, 646

Hasegawa, Y. & Ida, S. 2013, , 774, 146

Hashimoto, J., Aoyama, Y., Konishi, M., et al. 2020, arXiv e-prints, arXiv:2003.07922

Helled, R., Nettelmann, N., & Guillot, T. 2020, , 216, 38

Henning, T., Il'In, V. B., Krivova, N. A., Michel, B., & Voshchinnikov, N. V. 1999, , 136, 405

Henning, T. & Stognienko, R. 1996, , 311, 291

Hubeny, I. 1990, , 351, 632

Hubickyj, O., Bodenheimer, P., & Lissauer, J. J. 2005, , 179, 415

Isella, A., Benisty, M., Teague, R., et al. 2019, , 879, L25

Johansen, A., Oishi, J. S., Mac Low, M.-M., et al. 2007, , 448, 1022

Kataoka, A., Tanaka, H., Okuzumi, S., & Wada, K. 2013, , 557, L4

Keppler, M., Benisty, M., Müller, A., et al. 2018, , 617, A44

Klahr, H. & Kley, W. 2006, aap, 445, 747

Kley, W. 1998, , 338, L37

Kley, W., Bitsch, B., & Klahr, H. 2009, , 506, 971

Kley, W., D'Angelo, G., & Henning, T. 2001, , 547, 457

Kölligan, A. & Kuiper, R. 2018, , 620, A182

Kurokawa, H. & Tanigawa, T. 2018, , 479, 635

Lada, C. J. 2005, Progress of Theoretical Physics Supplement, 158, 1

Lagrange, A. M., Gratadour, D., Chauvin, G., et al. 2009, , 493, L21

Lambrechts, M. & Johansen, A. 2012, , 544, A32

Lambrechts, M., Johansen, A., & Morbidelli, A. 2014, aap, 572, A35

Lambrechts, M. & Lega, E. 2017, aap, 606, A146

Larson, R. B. 2003, Reports on Progress in Physics, 66, 1651

Lega, E., Crida, A., Bitsch, B., & Morbidelli, A. 2014, MNRAS, 440, 683

Levermore, C. D. & Pomraning, G. C. 1981, APJ, 248, 321

Lin, D. N. C. & Papaloizou, J. 1986a, , 307, 395

Lin, D. N. C. & Papaloizou, J. 1986b, apj, 309, 846

Lin, D. N. C. & Papaloizou, J. 1986c, , 309, 846

Liu, S.-F., Hori, Y., Müller, S., et al. 2019, , 572, 355

Lunine, J. I. 1993, , 31, 217

Machida, M. N., Kokubo, E., Inutsuka, S.-I., & Matsumoto, T. 2010, mnras, 405, 1227

Malygin, M. G., Kuiper, R., Klahr, H., Dullemond, C. P., & Henning, T. 2014, aap, 568, A91

Mamajek, E. E. 2009, in American Institute of Physics Conference Series, Vol. 1158, American Institute of Physics Conference Series, ed. T. Usuda, M. Tamura, & M. Ishii, 3–10

Manara, C. F., Morbidelli, A., & Guillot, T. 2018, , 618, L3

Masset, F. 2000, aaps, 141, 165

Mayor, M., Marmier, M., Lovis, C., et al. 2011, ArXiv e-prints [[arXiv]1109.2497]

Mayor, M. & Queloz, D. 1995, nature, 378, 355

McKinnon, W. B. 1987, Reviews of Geophysics, 25, 260

McNally, C. P., Nelson, R. P., Paardekooper, S.-J., & Benítez-Llambay, P. 2019, , 484, 728

Mesa, D., Keppler, M., Cantalloube, F., et al. 2019, , 632, A25

Mihalas, D. & Mihalas, B. W. 1984, Foundations of radiation hydrodynamics

Mizuno, H. 1980, Progress of Theoretical Physics, 64, 544

Mizuno, H., Nakazawa, K., & Hayashi, C. 1978, Progress of Theoretical Physics, 60, 699

Morbidelli, A., Lambrechts, M., Jacobson, S., & Bitsch, B. 2015, , 258, 418

Mordasini, C. 2014, aap, 572, A118

Mordasini, C., Klahr, H., Alibert, Y., Miller, N., & Henning, T. 2014, , 566, A141

Mordasini, C., Marleau, G.-D., & Mollière, P. 2017, aap, 608, A72

Movshovitz, N., Bodenheimer, P., Podolak, M., & Lissauer, J. J. 2010, , 209, 616

Müller, A., Keppler, M., Henning, T., et al. 2018, , 617, L2

Murray, C. D. & Dermott, S. F. 2000, Solar System Dynamics

Najita, J. R. & Kenyon, S. J. 2014, , 445, 3315

Nayakshin, S., Dipierro, G., & Szulágyi, J. 2019, , 488, L12

Ndugu, N., Bitsch, B., & Jurua, E. 2018, , 474, 886

Nelson, R. P., Papaloizou, J. C. B., Masset, F., & Kley, W. 2000, , 318, 18

Ogihara, M. & Hori, Y. 2018, , 867, 127

Ormel, C. W., Shi, J.-M., & Kuiper, R. 2015, , 447, 3512

Ossenkopf, V. & Henning, T. 1994, , 291, 943

Padoan, P., Haugbølle, T., & Nordlund, Å. 2014, , 797, 32

Pascucci, I., Testi, L., Herczeg, G. J., et al. 2016, , 831, 125

Pinte, C., Dent, W. R. F., Ménard, F., et al. 2016, , 816, 25

Piso, A.-M. A. & Youdin, A. N. 2014, apj, 786, 21

Piso, A.-M. A., Youdin, A. N., & Murray-Clay, R. A. 2015, , 800, 82

Pollack, J. B., Hollenbach, D., Beckwith, S., et al. 1994, , 421, 615

Pollack, J. B., Hubickyj, O., Bodenheimer, P., et al. 1996, icarus, 124, 62

Quanz, S. P., Amara, A., Meyer, M. R., et al. 2015, , 807, 64

Reggiani, M., Christiaens, V., Absil, O., et al. 2018, , 611, A74

Reggiani, M., Quanz, S. P., Meyer, M. R., et al. 2014, , 792, L23

Robert, C. M. T., Crida, A., Lega, E., Méheut, H., & Morbidelli, A. 2018, , 617, A98

Ronnet, T. & Johansen, A. 2020, , 633, A93

Ronnet, T., Mousis, O., Vernazza, P., Lunine, J. I., & Crida, A. 2018, aj, 155, 224

Sallum, S., Follette, K. B., Eisner, J. A., et al. 2015, , 527, 342

Sanchis, E., Picogna, G., Ercolano, B., Testi, L., & Rosotti, G. 2020, , 492, 3440

Scardoni, C. E., Rosotti, G. P., Lodato, G., & Clarke, C. J. 2020, , 492, 1318

Semenov, D., Henning, T., Helling, C., Ilgner, M., & Sedlmayr, E. 2003, aap, 410, 611

Shakura, N. I. & Sunyaev, R. A. 1973, , 500, 33

Simon, J. B., Armitage, P. J., Li, R., & Youdin, A. N. 2016, , 822, 55

Smith, B. A. & Terrile, R. J. 1984, Science, 226, 1421

Stahler, S. W., Shu, F. H., & Taam, R. E. 1981, , 248, 727

Stevenson, D. J. 1985, , 62, 4

Stone, J. M. & Norman, M. L. 1992, apjs, 80, 753

Szulágyi, J., Dullemond, C. P., Pohl, A., & Quanz, S. P. 2019, , 487, 1248

Szulágyi, J., Masset, F., Lega, E., et al. 2016, , 460, 2853

Takata, T. & Stevenson, D. J. 1996, , 123, 404

Tanigawa, T., Ohtsuki, K., & Machida, M. N. 2012, apj, 747, 47

Tanigawa, T. & Tanaka, H. 2016, , 823, 48

Teague, R., Bae, J., Bergin, E. A., Birnstiel, T., & Foreman-Mackey, D. 2018, , 860, L12

Tychoniec, Ł., Tobin, J. J., Karska, A., et al. 2018, , 238, 19

van Dishoeck, E. F. 2004, , 42, 119

Vazan, A. & Helled, R. 2020, , 633, A50

Wahl, S. M., Hubbard, W. B., Militzer, B., et al. 2017, , 44, 4649

Wahl, S. M., Wilson, H. F., & Militzer, B. 2013, , 773, 95

Williams, J. P., Cieza, L., Hales, A., et al. 2019, , 875, L9

Wilson, H. F. & Militzer, B. 2012, , 108, 111101

Wolszczan, A. & Frail, D. A. 1992, , 355, 145

Wong, M. H., Mahaffy, P. R., Atreya, S. K., Niemann, H. B., & Owen, T. C. 2004, , 171, 153

Wuchterl, G. 1991, , 91, 53

Zhu, Z., Ju, W., & Stone, J. M. 2016, apj, 832, 193

Acknowledgements

Anders, Bertram and Michiel, I am eternally grateful for all your guidance. Anders, I cannot understate my gratitude for your stamina in reading and re-reading, text-editing, and finding exactly that one crucial point in an argumentation that needs more work for it to become solid. Thank you for putting me through the AJ school of paper writing and science, even if it was a tough ride.
Bert, what more is there to say, I wish you all the pebbles in the sky! Thank you for being such a patient teacher of science.
Michiel, whenever there was a problem to discuss, your office was open. Those were fun times, thank you for them.
To Elena, for the best discussions about coding and science, and in the hope for many more meetings to come.
To Dainis, for all the interesting details about the history of astronomy in Lund and about life on Mars.
To Melvyn. While some might say that you are a bit super-communicative, you also make many good points. Those good points contributed greatly to me thinking about planet formation in a more galaxy-embedded context.
To my friends at the department, Adriaan, Simona, Giorgi, Katrin, Giorgi, Kalle, Linn, Eric, Abbas, Gregor, Thomas and Sebastian, I hope there will always be another coffee break to chat and have me sit grumpy around in the sunshine while you all play ping-pong.
To my parents, to whom this thesis is dedicated. Thank you for everything :)
My beyond-eternal gratitude to Urs, Katrin, my parents, Grażyna and Marcin Eckstein, Bert and Anders for proofreading.
To my friends which I made in Sweden, Anna, James, Arvid, Ellen, Gustav, Dragos, Carl,... I hope we never separate! A special thanks to Fiona, for telling me about the marshmallows.
Finally, to the astronomy department, sorry for eating all your core-hours!